Climatological study of boundary-layer air stagnation index for China and its relationship with air pollution

Qianqian Huang, Xuhui Cai, Jian Wang, Yu Song, Tong Zhu

College of Environmental Sciences and Engineering, State Key Joint Laboratory of Environmental Simulation and Pollution Control, Peking University, Beijing, 100871, China

Correspondence to: Xuhui Cai (xhcai@pku.edu.cn)

Abstract. Air stagnation index (ASI) is a vital meteorological measure of the atmosphere's ability to dilute air pollutants. The original metric adopted by US National Climatic Data Center (NCDC) is found not well suitable to China, because the decoupling between upper and lower atmospheric layer results in a weak link between the near surface air pollution and upper-air wind speed. Therefore, a new threshold for ASI—Boundary-layer air Stagnation Index (BSI) is proposed, consisting of daily maximal ventilation in the atmospheric boundary layer, precipitation and real latent instability. In the present study, the climatological features of BSI is investigated. It shows that the spatial distribution of the BSI is similar to the ASI; that is, annual mean stagnations occur most often in the northwest and southwest basins, i.e., Xinjiang and Sichuan basins (more than 180 days), and the least over plateaus, i.e., Qinghai–Tibet and Yunnan plateaus (less than 40 days). However, the seasonal cycle of the BSI is changed. Stagnation days under new metric are observed to be maximal in winter and minimal in summer, which is positively correlated with air pollution index (API) during 2000–2012. The correlations between BSI and concentration of fine particulate matter ($PM_{2.5}$) during January 2013 and November to December in 2015–2017 of Beijing are also investigated. It shows that the BSI matches the day-by-day variation of $PM_{2.5}$ concentration very well and is able to catch the haze episodes.

1. Introduction

Air pollution has attracted considerable national and local attention and become one of the top concerns in China (e.g., Chan et al., 2008; Guo et al., 2014; Huang et al., 2014; Peng et al., 2016). It is also a worldwide problem, shared by the United States, Europe, and India, etc (e.g., Lelieveld et al., 2015; van Donkelaar et al., 2010; Lu et al., 2011). The initiation and persistence of air pollution episodes involve complex processes, including direct emissions of air pollutants, and secondary formation by atmospheric chemical reactions, etc. Meteorological background is also significant for its ability to affect the accumulation and removal or dispersion of air pollutants (e.g., Tai et al., 2010; Chen and Wang, 2015; Dawson et al., 2014). A substantial number of studies have been

carried out on the abnormal meteorological conditions during haze events. They suggested that a persistent or slow moving anti-cyclone synoptic system inclines to forms a haze episode (Ye et al., 2016; Leibensperger et al., 2008; Liu et al., 2013; Yin et al., 2017). Besides the driving force from synoptic scale, some local meteorological conditions are also favorable for heavy air pollutions. Low atmospheric boundary layer (ABL) height can act as a lid to confine the vertical mixing of air pollutants (Zhang et al., 2010; Ji et al., 2012; Bressi et al., 2013). Light winds lack the ability to disperse air pollutants or transport them far away (Fu et al., 2014; Rigby and Toumi, 2008; Tai et al., 2010), and those pollutants blown by winds could directly contaminate the downwind zone (Wehner and Wiedensohler, 2003; Elminir, 2005). In addition, high relative humidity usually results in low visibilities through aerosol hygroscopic growth (Chen et al., 2012; Quan et al., 2011). Studies have shown that haze pollutions in China occurs more frequently over the past decades, especially those in the eastern region (Wang and Chen, 2016; Pei et al., 2018). Apart from increased emissions of pollutants, climate change also plays an important role in air pollution intensification. Less cyclone activities and weakening East Asian winter monsoons (Pei et al., 2018; Yin et al., 2017) resulted from the decline of Arctic sea ice extent (Deser et al., 2010; Wang and Chen, 2016) and expanded tropical belt (Seidel et al., 2008) are believed to bring about more stable atmosphere in eastern China and cause more haze days (Wang et al., 2015). Hence, the analysis of meteorological background related to air pollution is of great importance.

Researchers have developed many indexes comprised of different meteorological variables to describe the ability of transport and dispersion of the atmosphere. For example, Cai et al. (2017) constructed haze weather index with 500 hPa and 850 hPa wind speeds and temperature anomalies between 850 hPa and 250 hPa. Han et al., (2017) proposed air environment carrying capacity index including air pollutants concentration, precipitation and ventilation coefficient. Among these indexes, air stagnation index (ASI), consisting of upper- and lower-air winds and precipitation, is in use till today. The US National Climatic Data Center (NCDC) monitors monthly air stagnation days for the United States since 1973 to indicate the temporal buildup of ozone in the lower atmosphere (http://www.ncdc.noaa.gov/societal-impacts/air-stagnation/). A given day is considered stagnant when the 10 m wind speed is less than 3.2 m/s (i.e., near surface wind is insufficient to dilute air pollutants), 500 hPa wind speed less than 13 m/s (i.e., lingering anti-cyclones, indicating weak vertical mixing), and no precipitation occurs (i.e., no rain to wash out the pollutants) (Korshover, 1967; Korshover and Angell, 1982; Wang and Angell, 1999; Leung and Gustafson, 2005; Horton et al., 2014). Perturbation studies have proven that air stagnation positively correlates with ozone and particulate matter concentrations (e.g., Liao et al., 2006; Jacob and Winner, 2009).

Huang et al. (2017) followed the NCDC's metric of air stagnation and investigated the climatological mean features of it for China. It was found that the spatial distribution of annual mean stagnations is in good agreement with that of air pollution index (API). Basins in Xinjiang and Sichuan provinces are reported to experience heavy air pollutions most often (Mamtimin and Meixner, 2007; Wang et al., 2011; Chen and Xie, 2012; Li et al., 2015), and according to Huang et al. (2017), these two basins were identified as regions with most frequent stagnation occurrence (50% days per year). However, the seasonal variation pattern of air stagnation barely correlated with that of API. Stagnations happen the most frequently in summer and the least in winter, whereas the API has the opposite seasonal pattern (Li et al., 2014). Why does the NCDC criteria fail to represent it? As the mid-tropospheric wind is the main driving force of air stagnations (Huang et al. 2017), we analyzed the 500 hPa wind speed in the most polluted days of Beijing when their API ranks in the 90^{th} percentile or higher in the autumn and winter seasons of each year during 2000–2012 (Fig. 1). It is found that in 75% of the most polluted days, the 500 hPa wind speed is stronger than 13 m/s. It suggests that air pollutions do not necessarily link with weak upper-air wind speed, and thus weak 500 hPa wind speed is not an appropriate indicator for pollution occurrence.

In order to address this deficiency, Wang et al. (2017) tried to modify ASI by taking 10 m wind speed, ABL height and the occurrence of precipitation into consideration. Their air stagnation threshold is determined by a fitting equation which relates to $PM_{2.5}$ concentration, 10 m wind speed and ABL height. This equation varies with locations and changes over time. In this study, we propose a new air stagnation identification—Boundary-layer air Stagnation Index (BSI). Instead of relating this index directly to air pollution monitoring data, we put the thresholds on meteorological basis only and hope that BSI is more universal and robust in principle. The BSI metric retains no-precipitation threshold to exclude wet deposition, gives up upper-air wind speed, replaces 10 m wind speed with ventilation in the ABL to represent both the horizontal dilution and vertical mixing scale of the atmosphere, and takes real latent instability of the surface atmosphere into consideration. The components of BSI are introduced one by one in the following except precipitation threshold.

The depth of ABL is of much concern in air pollution studies, since it acts as the vertical mixing confinement of air pollutants, and in turn, determines surface concentrations of them. The ABL depth normally shows a diurnal cycle: a minimum at night and maximum in the afternoon (Stull, 1988). So is the vertical mixing extent of air pollutants. On the other hand, the strength of horizontal dilution (i.e., transport wind speed) is also significant in atmospheric dispersion and presents a similar diurnal pattern as ABL height. For the consideration of environmental capacity, mixing layer depth (MD) and transport wind in the afternoon are of great importance since they together

represent the best dilution condition during the entire day (Holzworth, 1964; Miller, 1967). Therefore, ventilation in the maximum MD (referred to as ventilation hereinafter) is adopted in the BSI as a mixture to simultaneously indicate the largest extent of horizontal dilution and vertical mixing.

MD is not a quantity of routine meteorological observation (Liu and Liang, 2010). It is usually derived from profiles of the temperature and wind speed/direction as well as humidity from local and short-term observation project or experiment (Seibert et al., 2000). The methods used to detect or estimated MD includes: observation of sodar (Beyrich, 1997; Lokoshchenko, 2002), lidar (Tucker et al., 2009), ceilometer (Eresmaa et al., 2006; van der Kamp and Mckendry, 2010), wind profiler (Bianco and Wilczak, 2002), etc. Holzworth (1964, 1967) pioneers the work to obtain long term, large area maximum MD (MMD) information by "parcel method", in which MMD is interpreted as the height above ground of dry adiabatic intersection of the maximum surface temperature during the daytime with the vertical temperature profile from morning (1200 UTC for China) radiosonde observation. Seidel et al. (2010) compared MMD results from parcel method along with six other methods using long-term radiosonde observations, and concluded that climatological MMD based on parcel method is warranted for air quality studies. Their further work (Seidel et al. 2012) compared the results derived from sounding data with other climate models, and provided a comparison of the MD characteristics between North America and Europe. These two studies lay the groundwork for the global climatology of MD. Since then, the climatological characteristics of MD over regional (e.g., for Swiss plateau by Coen et al. (2014), for Indian sub-continent by Patil et al. (2013)) or global scales have been investigated (Von Engeln and Teixeira, 2013; Ao et al., 2012; Xie et al., 2011; Jordan et al., 2010).

MMD derived from parcel method is recommended for air pollution potential evaluation. However, in the presence of clouds, it agrees well with the depth of cloud base (Seidel et al., 2010), which is lower than the actual magnitude of vertical mixing extent of air pollutants. In order to compensate for this deficiency, we take the thermo-dynamical parameter convective available potential energy (CAPE) into consideration, implying the energy of ascension from the base to top of the cloud (Riemann-Campe et al., 2011). CAPE denotes the potential energy available to form cumulus convection and thus serves as an instability index (Blanchard, 1998). It is a measurement of the maximum kinetic energy per unit air mass achieves through rising freely from the level of free convection (LFC) and the level of neutral buoyancy (LNB) (i.e., bottom and top of the cloud), since the virtual temperature of the buoyant parcel is higher than that of its environment (Markowski and Richardson, 2011). Holton (1992) indicated that when buoyancy is the only force of an air parcel, CAPE corresponds to the upper limit for the vertical component of the

velocity, as $CAPE = w_{max}^2 / 2$. However, high values of CAPE do not necessarily lead to strong convection (Williams and Renno, 1993). Its opposing parameter convective inhibition (CIN) describes the energy needed by the rising air parcel to overcome the stable layer between the surface and LFC (Markowski and Richardson, 2011; Riemann-Campe et al., 2009). CAPE stored in the atmosphere is activated if the value of CAPE is larger than that of CIN, that is, under real latent instability conditions. Therefore, climatological study of CAPE and CIN provides an insight into the strength of atmospheric convection (Monkam, 2002).

In sum, unfavorable meteorological variables are critical to the occurrence of air pollution episodes. ASI from NCDC is designed to evaluate the air dilution capability, but is found to be inappropriate for China. So we propose a new stagnation index BSI instead. Our aim in the present work is to investigate the climatological features of the BSI, as well as its components, and examine the practicability of the BSI by studying its relationship with air quality monitoring data, i.e., API data during 2000–2012, and concentrations of fine particulate matter ($PM_{2.5}$) in January 2013 of Beijing.

2. Data and Methodology

2.1 Data

2.1.1 Meteorological data

Radiosonde data are used to calculate the daily ventilation. Soundings from all the international exchange stations across China (95 stations) for the 30-year period (1985–2014) were obtained from the archive of the University of Wyoming (available at http://weather.uwyo.edu/upperair/sounding.html). This dataset provides twice daily (0000 and 1200 UTC) atmospheric soundings, including the observed temperature, geopotential height, and wind speed data at pressure levels, as well as additional derived variables CAPE and CIN.

Surface observational data are used to identify daily maxima of surface air temperature. We extracted hourly observations of surface air temperature during 1985 to 2014 from Integrated Surface Database (ISD), provided by NCDC. Data are accessible from FTP (ftp://ftp.ncdc.noaa.gov/pub/data/noaa). The entire ISD archive has been previously processed through quality control procedures by NCDC, including algorithms checking for extreme values and limits, consistency between parameters, and continuity between observations. More detailed information regarding the quality control process can be found at https://www.ncdc.noaa.gov/isd.

Long-term (1985–2014) daily precipitation data were collected from China Meteorological Administration (CMA). These data are available at http://data.cma.cn/data/detail/dataCode/SURF_CLI_CHN_MUL_DAY_CES_V3.0.html.

For any investigation, we limited the study to the stations where the all quantities—radiosondes, surface temperature observations and daily precipitation data—are available together. Therefore, air stagnations of 66 stations are analyzed in this study. Figure 2 shows that these 66 stations are fairly spread all over the contiguous China, except that the Qinghai–Tibet Plateau particularly the western Tibet is not well sampled.

We conducted a general survey of the availability of valid data (radiosonde data, daily maximum temperature, and daily precipitation are valid at the same time) for each of the 66 stations (Appendix A). It shows that among these 66 stations, datasets of 62 stations are available from January 1985 to December 2014, while datasets of the other 4 stations (Wenjiang, Jinghe, Chongqing, Shanghai) cover less than 30 years. The shortest duration is 9 years at Wenjiang station. The percentage of valid data are more than 96% of each station. In conclusion, the datasets are sufficient for us to conduct a climatological study of the BSI on a countrywide basis.

2.1.2 Air quality data

To discuss the practical applicability of the BSI, daily API data (available at http://datacenter.mep.gov.cn) of four representative stations (Harbin, Urumqi, Beijing and Chongqing) during 2000–2012 are used. In order to exclude the influences of emission variations and chemical reactions to the greatest extent, and focus on the effects of meteorological conditions, we only analyse API data on those days when the primary pollutant is $PM_{2.5}$. The concentration of $PM_{2.5}$ is also used as another good metric for air pollution. We collected 24-h averaged $PM_{2.5}$ concentrations of Beijing during November to December in 2015, 2016 and 2017 from Ministry of Environmental Protection (MEP) of China. The concentrations during January 2013 are not yet accessible from MEP, so we obtained the hourly data from US Embassy instead. With these concentrations, we conducted case studies and examined the ability of the BSI to track day-by-day variation of air pollution.

2.2 Method

2.2.1 Daily MMD and ventilation

The parcel method (Holzworth, 1964) are used to calculate daily MMD. There are two steps in this calculation: 1) identify the daily maximum surface air temperature from hourly temperature data during 0800 to 2000 Beijing standard time (BJT; UTC+8); 2) starting from the maximal surface temperature, a dry-adiabatic line extends to intersect the temperature profile of morning sounding. Then the intersection height above ground level is MMD. Since the vertical resolution is coarse (10^1–10^2 m), the data of temperature from radiosonde were interpolated linearly to height levels with 1-m vertical resolution. It is noticed that the parcel method may fail to determine the MMD sometimes when the temperature profile itself is close to a dry-adiabatic line (Lokoshchenko, 2002), or the height corresponding to the first valid value of the temperature is too high. These cases are treated as missing data and ignored.

Wind speeds at 1200 UTC (i.e., 2000 BJT) from radiosonde were also interpolated linearly to height levels with 1-m resolution, and ventilation is derived by integrating the wind speeds from surface to the top of the maximum mixing layer:

$$vent = \int_0^{MMD} u(z)dz\,, \tag{1}$$

where $vent$ is short for ventilation, z is the elevation above surface, $u(z)$ is the wind speed at z m above the ground. Ventilation is a direct measure of the dilution capacity of the atmosphere within the ABL. Higher values of ventilation indicate effective dilution.

From Equation (1), the average value of the wind speed through the MMD, i.e., the transport wind speed (U_T) writes:

$$U_T = {vent}/{MMD}\,. \tag{2}$$

2.2.2 CAPE and CIN

The values of CAPE and CIN are taken directly from the sounding files provided by University of Wyoming. Based on pseudo-adiabatic assumption, the formula for CAPE calculation (Murugavel et al., 2012) is:

$$CAPE = g\sum_{LFC}^{LNB}\frac{\Delta z(T_{vp}-T_{ve})}{T_{ve}}, \quad (3)$$

where T_{vp} designates the virtual temperature of lifted air parcel of the lowest 500 m of the atmosphere, T_{ve} is virtual temperature of the environment, Δz is incremental depth and g is gravitation constant. Only values of CAPE calculated from 1200 UTC (i.e., 2000 BJT) profiles are considered for this analysis, representing the maximum convective potential energy of the day.

The value of CAPE is sensitive to the calculation method, such as the treatment of the freezing process (Williams and Renno, 1993; Thompkins and Craig, 1998; Frueh and Wirth, 2007). However, climatological mean features of CAPE are not sensitive to the calculation method if one particular method is applied throughout (Myoung and Nielsen-Gammon, 2010; Murugavel et al., 2012). Therefore, our results are assumed to be insensitive to the method of CAPE calculation.

CIN is calculated through:

$$CIN = -g\sum_{Zsurface}^{LFC}\frac{\Delta z(T_{vp}-T_{ve})}{T_{ve}}. \quad (4)$$

It should be noted that values of CIN in the following discussion all refer to the absolute values of CIN.

2.2.3 Criteria for the BSI

The BSI is designed to better describe the atmospheric dispersion capability in ABL. A given day is considered stagnant when the value of daily maximum ventilation is less than 6000 m^2/s (Holzworth, 1972), the value of CAPE is less than that of CIN, and daily total precipitation is less than 1 mm (i.e., a dry day). The definition of air stagnation case is retained: 4 or more consecutive air stagnant days are considered as one air stagnation case (Wang and Angell, 1999). In order to show the spatial distribution of stagnation days and cases over continental China, results of 66 stations have been interpolated in space on the $2°\times 2°$ grid by cubic splines.

3. Climatology of the BSI components: ventilation, precipitation, and real latent instability

3.1 Ventilation climatology

The daily maximal ventilation condition is distributed with substantial regional heterogeneity (Fig. 3a). It is shown that ventilation might be the largest (more than 15000 m^2/s) over Qinghai–Tibet Plateau, which is the world's highest plateau with an average elevation exceeding 4500 m. The areas neighboring to the plateau, Yunnan Plateau and Inner Mongolian Plateau, also experience relative large ventilation (10000–15000 m^2/s). However, the south of China, where the population and industry are dense, exhibits the most unfavorable atmospheric ventilation conditions, especially the Sichuan Basin where the ventilation is lower than 4000 m^2/s.

Ventilation is a combined response of both the MMD and transport wind speed. It is noticed that regions with high ventilation also experience relatively high MMD and strong transport wind, whereas regions with poor ventilation conditions also exhibit low MMD and weak transport wind (Fig. 3). First of all, large MMD (more than 2000 m) is observed over Qinghai–Tibet–Yunnan Plateau, whereas low MMD (about 1000 m or less) locates in the southeast China (Fig. 3b). This distribution pattern is interpreted as the effect of terrain. High terrain elevation corresponds to thinner air and lower value of aerosol optical thickness, less precipitable water vapor amount, and stronger solar radiation (Chen et al., 2014; Zhu et al., 2010), which enhance thermal convections and lead to high MMD. The results agree with the recent study of Liu et al. (2015). Secondly, the plateau locates right in the westerlies, and it can even break the jet stream into two branches surrounding the northern and southern edges of the plateau. Therefore, as Schiemann et al. (2009) revealed, the transport wind is strong (more than 6 m/s) over plateaus (Fig. 3c) because of the combined influence of westerly jet and elevated topography, and weak (less than 4 m/s) over Xinjiang and Sichuan basins. Based on the analyses above, the results over Tibetan Plateau are considered reasonable, although observation stations are sparse there.

Generally, most regions of China experience a good ventilation condition in spring (Fig. S1). Specifically, different regions show different seasonal variation patterns. Four representative stations (Harbin, Urumqi, Beijing and Chongqing; shown in Fig. 2 as crosses) are selected to analyze the monthly variation of ventilation, as well as the corresponding MMD and transport wind speed (Fig. 4). It is shown that patterns of the monthly variation of ventilation are different at different stations. Ventilations of Harbin and Beijing reach a peak in April, followed by a rapid fall to a low value in August. Subsequently, these values increase to a secondary peak in October and then decrease to the minima in January. Correspondingly, MMD and transport wind speed also show a bimodal

distribution pattern with two peaks: one in spring and another in autumn. For the north China, solar radiation is strong in summer; but significant rains and cloudy skies restrict the thermal convective processes and keep the MMD to a low value in monsoon season. In addition, the wind speed is typically weaker in summer and stronger in winter (Frederick et al., 2012). However, the winter solar radiation is weak and constrains the development of atmospheric boundary layer. Consequently, weak transport wind and poor ventilation are observed in both summer and winter. The seasonal behavior of ventilation conditions of Urumqi is different. The monthly mean value of ventilation presents a unimodal distribution with the mean value ranging from 788 m^2/s (January) to 15544 m^2/s (June) through the year. The corresponding MMD and transport wind speed also show similar seasonal behavior, ranging from 334 m and 2.2 m/s in January to 2406 m and 6.2 m/s in June, respectively. This may be attributed to the unique local climate of northern Xinjiang, where the climate is considered as semi-arid steppe (Peel et al., 2007). In Urumqi, short summer and long winter are the dominate seasons while spring and autumn are only transitional ones (Domroes and Peng, 1988). Monthly precipitation averaged over the recent 30 years (1985–2014) ranged between 12.2 mm (January) and 39.9 mm (May), demonstrating the arid climate of Urumqi (shown later in Fig. 6). The lack of precipitation (especially in summer) may lead to a unimodal distributed MMD and ventilation condition in Urumqi. Apart from its one-peak pattern, the transport wind speed in Urumqi is weaker than that in Harbin and Beijing, owing to the block of Qinghai–Tibet Plateau in the south. Chongqing, on the other hand, is an extreme example, where atmospheric ventilation is poor (lower than 10000 m^2/s) throughout the year. Along with this are low MMD (lower than 1500 m) and weak transport wind (weaker than 4 m/s). This natural situation may put large pressure on local air quality.

3.2 Precipitation climatology

Another component for the BSI is precipitation, which is retained from the metric for ASI. Figure 5 shows that the rainfall amount and rainy days are observed to be more significant over the southeast of China than inland areas due to the transport of moisture from the ocean by summer monsoon (Fig. S2). Rainfall amount and rainy days of four representative stations (Harbin, Urumqi, Beijing and Chongqing) are shown in Fig. 6. It is seen that generally, Chongqing experiences the largest annual rainfall amount and Urumqi the least (Fig. 6a). Seasonally, rainfall is abundant in the summer monsoon season and scarce in winter for Harbin, Beijing and Chongqing. But for Urumqi, it keeps a low value throughout the year, illustrating the arid climate in the northwest of China. As for the rainy days, Harbin and Beijing experience the most of them in summer monsoon season, sharing the similar unimodal pattern with their monthly rainfall amount. Rainy days of Urumqi keep a low value all the year round, the same as

the pattern of its rainfall amount. However, the variation of rainy days (Fig. 6b) of Chongqing shows two distinct peaks: one is seen in May and June (about 12 days) and another in October (about 11 days). It indicates that autumn in Chongqing is characterized by moderate rain with more frequency.

3.3 CAPE and CIN climatology

Apart from the actual rainfall to washout air pollutants, CAPE values are also important since it relates to convection initiations and thermodynamic speed limit (Markowski and Richardson, 2011). Larger values of CAPE with CIN deducted (referred to as CAPE_CIN hereinafter) mean a higher probability in the destabilization of the atmosphere and genesis of stronger wet convection.

Annual mean values of CAPE (Fig. 7a) generally increase from south to north, following the spatial distribution of the near-surface specific humidity and temperature (Riemann-Campe et al., 2009 and their Fig. 2). The maxima occur in the southern coastal areas (larger than 300 J/kg), where the surface temperature is high and moisture is abundant. There is also large CAPE stored in the atmosphere over the southern region of Qinghai–Tibet Plateau. As the summer monsoon of south Asia is established, warm moist air originating from the Bay of Bengal is blown to Tibet plateau (Romatschke et at., 2010), and hence large value of CAPE exists. The minimal CAPE values are observed in the north especially the northwest i.e., the arid and relatively cold regions, where the value of CAPE is less than 30 J/kg. In contrast to relatively large values of CAPE, values of CIN over China range from 4 to 70 J/kg (Fig. 7b). Smaller values of CIN occur in the same region where smaller CAPE values are observed. Large CIN values are observed in Sichuan basin, indicating the need of stronger forcing to overcome stable atmospheric layer for the occurrence of a wet convection. As a variable indicating real latent instability, annual mean CAPE_CIN (Fig. 7c) is spatially distributed similarly to CAPE. In general, smaller values are observed in the northwest of China (less than 10 J/kg) and larger values occur in the southmost part of the country and south of Qinghai–Tibet Plateau (larger than 300 J/kg).

Generally, the value of CAPE_CIN is largest in summer (Fig. S3). The annual cycles of CAPE and CIN of four representative stations (Harbin, Urumqi, Beijing and Chongqing) are investigated (Fig. 8). CAPE values present a unimodal distribution. They generally increase in spring, achieve maxima in summer months, then begin to decrease during autumn season and reach minima in winter. The annual cycle of CIN of Harbin, Beijing and Chongqing displays a similar distribution as that of CAPE but not as pronounced. As a result, CAPE of these three

stations are much larger than the corresponding CIN during spring, summer and autumn. Chongqing presents the largest value of CAPE and CAPE_CIN, indicating the largest probability to form cumulus convection. In contrast, CIN value of Urumqi is comparable to its CAPE. Both of them are very small, ranging from 0 to 50 J/kg. In addition, the value of CIN is less than or almost equal to CAPE in autumn and winter months. Under such circumstances, destabilization will not occur, even if the layer has been lifted sufficiently.

4. Climatological Results of the BSI

The national distribution of annual mean the BSI during 1985–2014 is displayed in Fig. 9. Results show that the spatial distributions of boundary-layer air stagnation days and cases are basically consistent with the old ones displayed in Huang et al. (2017). The new stagnation days and cases are still prevalent over Xinjiang and Sichuan basins (more than 180 days and 14 cases per year) and barely occur over Qinghai–Tibet and Yunnan plateaus (less than 40 days and 2 cases per year). However, the distribution pattern of the duration of one stagnation case is changed under new criteria. Air stagnation cases persist longer in the north part of China (more than 8 days) and then the central part (about 7 days). The longest duration is observed in the northwest region of China (more than 10 days), instead of the south of this country in the earlier study (Huang et al., 2017). The shortest duration occurs over Qinghai–Tibet and Yunnan plateaus (less than 5 days).

Much improved are the seasonal cycles of air stagnation days and cases. Generally, boundary-layer stagnant conditions occur the most frequently in winter and the least in summer (Fig. S4). Results of monthly variations of four representative stations (Harbin, Urumqi, Beijing and Chongqing), as well as the national averages, are displayed in Fig. 10. It is shown that stagnation days under ASI metric is more in summer and less in winter. According to Huang et al. (2017), the behavior of upper-air wind speeds is the main driver of the ASI distribution. A weaker latitudinal pressure gradient at the upper layer of the atmosphere results in more air stagnation occurrences in summer. In contrast, the BSI is observed to be maximum in winter and minimum in summer. This behavior results from the cumulative responses of its components. We use standardized partial regression coefficients from multiple linear regression analysis to determine which variable is more important to BSI results (Table 1). It is shown that during the wintertime of Harbin, Urumqi and Beijing, ventilation is the main driver of BSI; precipitation contributes less; and cumulus convection barely plays a part in BSI results. In summer, however, ventilation and cumulus convection both contribute a lot. For Harbin, they play an almost equal role, with regression coefficients of 0.57 and 0.48 respectively. For Beijing, the contribution of CAPE out weights that of ventilation

more than twice. For Urumqi which is in the semi-arid climate region, the ventilation is still the main driver of BSI behavior (β =0.83), while precipitation and CAPE contribute equally (β =0.36 and 0.4 respectively). The characteristics in Chongqing is different from the other three stations. With more convective energy stored in the atmosphere (Fig. 8), the seasonal variation of BSI relies more on CAPE: it is the second contributor during winter and spring (β =0.36 and 0.38 respectively), and becomes the main contributor in summer and autumn (β =0.75 and 0.68 respectively). Noticeably in summer, the BSI is dominated by cumulus convection, while the ventilation barely plays a role. The intention we add CAPE/CIN into the criteria is to make up for the deficiency of daily maximum mixing layer depth (MMD) derived from parcel method failing to describe the convection between the cloud base and cloud top. So it is expected that CAPE/CIN plays a more important role in summer.

5. Correlations between the BSI and actual air pollution

API as an indicator of air quality is used to testify the reasonability of the BSI. Figure 11 shows that, monthly variations of the BSI can basically represent the annual cycles of API. For all the four representative stations, the annual cycle of boundary-layer air stagnation days reach maxima in winter and minima in summer, in agreement with the annual cycle of API. However, there are two failures for the BSI to predict the API. One is the secondary peak of API in spring for both Beijing and Harbin, the BSI cannot represent it. This is attributed to the influence of sand storms in spring in northern China. Sand storms usually result in high level of particulate air pollution (high API), and are accompanied by strong winds and good ventilation conditions (low BSI). Another discrepancy is that the BSI during October to December of Urumqi is equally poor, whereas the corresponding API grows significantly during these three months. We cannot explain this discrepancy till now. The ASI is also shown in Fig. 11. Obviously, the BSI performs much better in indicating actual air pollution levels.

The correlations between monthly mean API and the total air stagnation days in this month are also investigated (Fig. 12). In order to exclude the impact of seasonal variation in source strengths, the investigation only covers data of winter half-year (i.e., October–March) when domestic heating in north China leads to more energy consumption and more serious air pollution pressure. With only data of winter half-year analyzed, stagnation days under the BSI metric are generally larger than those under the ASI, since the occurrence of BSI is more frequently in winter and less in summer, while the ASI is the opposite (Fig. 10). Figure 12 shows that with the ASI criteria, monthly mean API has no evident correlation with monthly stagnation days, or even decrease with them (Chongqing), which is clearly irrational. Instead, with the BSI criteria, monthly mean API basically increase with the number of boundary-

layer stagnation days as we expected.

In addition, we have also explored the ability of the BSI to capture the air pollution days (Table 2). Every day during 2001–2012 is classified according to its API value. Then we calculated how many days in one category are considered as air stagnation day, under the ASI and BSI criteria. Results show that for moderate air quality with API ranging from 50 to 100, the number of stagnation days that identified by the BSI is almost the same as or even less than that by the ASI. For unhealthy air quality with API ranging from 101 to 500, the percentage of identified air stagnation days with the BSI is basically more than that with the ASI, the former may even double or triple the latter in some situation. It suggests that the BSI has reduced the probability of misjudging an air pollution day and increased the chances to capture the true one.

Apart from the statistical analysis of correlations between the API and BSI, we also conducted a case study about $PM_{2.5}$ concentrations and BSI (Fig. 13). It is found that the BSI is able to track the day-by-day variation of air pollution episode in January 2013 in Beijing, which was characterized by continuous high $PM_{2.5}$ concentrations (Ji et al., 2014; Sun et al., 2014). The mean daily $PM_{2.5}$ concentration during that month ranged from 15.8 (January 1) to 568.6 (January 12) $\mu g/m^3$. There were only three days when the $PM_{2.5}$ concentration reached the standard of less than 25 $\mu g/m^3$ for 24 h average suggested by the Air Quality Guidelines (AQG) of the World Health Organization (WHO; WHO 2005), and only seven days met the China National Ambient Air Quality Standards (CNAAQS; 75 $\mu g/m^3$ for 24 h average). In particular, the record-breaking hourly concentration of $PM_{2.5}$ reached as high as 886 $\mu g/m^3$ at 1900 local time on January 12, exceeding more than 11 times the CNAAQS and 35 times the WHO AQG.

Ordinarily, emissions from one particular region remain constant over a short period. Therefore, the day-by-day variation of local air quality mainly depends on its weather conditions. Hourly concentration of $PM_{2.5}$ of Beijing and air stagnation days during January 2013 are presented in Fig. 13, as well as the components of both ASI and BSI. According to weather records, no precipitation is reported in this month except on January 20 and 31. In addition, the values of CAPE and CIN are nearly zero in winter season, as mentioned above. Therefore, we only focus on the ventilation condition of the BSI, and 500 hPa and 10 m wind speeds of the ASI. It is seen that there are two long-duration haze episodes, i.e. January 10–14 and 25–30, and some minor $PM_{2.5}$ concentration peaks in January 6–7, 16, 18–19, and 21–23 during this month. The ASI only successfully captures one heavy pollution in January 29 and one moderate pollution in January 21. But it fails to capture other heavily polluted days, and

misjudges a clean day (January 3) as a pollutant accumulation day. The reason is that although 10 m wind speed falls below the 3.2 m/s standard since January 3, 500 hPa wind speed—the dominant component in the ASI (Huang et al., 2017)—is generally above the 13 m/s standard except for January 3, 21 and 29. It verifies again that 500 hPa wind speed is not appropriate to be an ASI element. The boundary-layer air stagnation pattern matches the day-by-day variation of $PM_{2.5}$ concentration pretty well. The two major and four minor haze episodes are all successfully identified as boundary-layer air stagnation day except January 11. It should be reasonable since even though the daily mean concentration of $PM_{2.5}$ on January 11 was relatively high, its hourly concentration actually decreased throughout the day. Correspondingly, this day presents a good ventilation condition (9328 m^2/s; Fig. 13b) and is identified as a non-stagnation day.

We also investigated the time series of daily $PM_{2.5}$ concentration in Beijing during November and December in 2015, 2016 and 2017, as well as the stagnation days under ASI and BSI metric (Figure 14), to further demonstrate the performance of BSI. It is shown that the BSI is a better metric to capture the meteorological conditions conductive to poor air quality. Nearly all the peaks of $PM_{2.5}$ concentration or its accumulating processes correspond to boundary-layer stagnant days. Compared to 2015 and 2016, $PM_{2.5}$ concentration during November and December in 2017 was significantly reduced. The 24-averaged $PM_{2.5}$ concentration was less than 50 $\mu g/m^3$ in 70% days and larger than 150 $\mu g/m^3$ in only three days. Correspondingly, boundary-layer stagnant days were greatly reduced, especially stagnant cases. Less stagnant cases mean smaller meteorological potential for air pollutants to accumulate. As a result, air quality during the late autumn and early winter in 2017 was largely improved. Figure 15 shows that the averaged concentration of $PM_{2.5}$ during these two months in 2015, 2016 and 2017 negatively correlates to the number of boundary-layer stagnation days. It illustrates that an increase in the capacity of atmospheric environment plays an important role in air quality improvement during November and December in 2017, and BSI successfully represents this trend.

However, we do not expect that BSI can perform well in capturing air pollution episodes in spring and summer. The reason is that this metric only indicates adverse meteorological condition to air pollution, without the influences of emissions or chemical reactions in the atmosphere. In spring, air quality of Beijing is greatly deteriorated by frequent sand storms (He et al., 2001), which are often accompanied by strong winds and good ventilation conditions (low BSI). This results in great discrepancies between BSI and actual air quality (Fig. 11). During summer, highly oxidative atmosphere and secondary formation of aerosols are main problems (Fu et al., 2014; Ran et al., 2011). As a result, BSI may not be able to track the actual air pollution episodes during these two seasons.

6. Conclusion

Meteorological background is critical to the occurrence of air pollution events, since it determines the accumulation or dilution of air pollutants. The United States adopts air stagnation index (ASI) to measure the meteorological state, taking 500 hPa and 10 m wind speeds, and precipitation into consideration. However, this metric is found not well adequate for China. Taking Beijing as an example, strong upper-level wind occurs in 75% of most polluted days (API ranks in the 90th percentile or higher). It means that strong upper-air winds does not necessarily drive the near surface dispersion of air pollutants. In the present study, we proposed a new metric for ASI—Boundary-layer air Stagnation Index (BSI), based on (i) daily maximal ventilation, indicating horizontal dilution and vertical mixing extent in the boundary layer, (ii) real latent instability, implying the convection between the layer of cloud base and cloud top, (iii) precipitation, representing the washout effects of air pollutants.

Based on sounding data and hourly near-surface temperature observations, we firstly calculated daily maximum mixing layer depth during 1985–2014, and then estimated daily maximal ventilation in the boundary layer. Combined with daily precipitation and CAPE and CIN values, we derived results of the BSI of 66 stations across the country, and investigated the climatological features of them. It shows that the BSI keeps a similar spatial pattern in comparison with the ASI (Huang et al., 2017). Annual mean stagnation days under BSI metric are most prevalent (more than 180 days) over the northwest and southwest basins, i.e., Xinjiang and Sichuan basins, and least (less than 40 days) over Qinghai–Tibet and Yunnan plateaus. However, the annual cycle of the boundary-layer stagnation days is different, with the frequency of stagnation occurrences reaching a maximum in winter and minimum in summer, which is contrary to the ASI result. The seasonal variation of BSI is the cumulative response of its components (ventilation, precipitation and cumulus convection). It is dominated by ventilation coefficient during winter and influenced by the combined results of all components in summer.

The annual cycle of boundary-layer stagnation days is in consistent with the monthly variation of API during 2000–2012. Moreover, the BSI shows a positive correlation with API during boreal winter half-year, and is found to be more efficient to identify unhealthy air quality with API ranging from 101 to 500. In addition, the BSI also well track the day-by-day variation of $PM_{2.5}$ concentration during the record-breaking haze episodes in January 2013 in Beijing and successfully represent the improved air quality during November and December in 2017. Therefore, the BSI may act as a better indicator of atmospheric dispersion and dilution in air pollution research.

Acknowledgements

This work is partially supported by National Natural Science Foundation of China (41575007, 91544216) and Clean Air Research Project in China (201509001). We greatly acknowledge the work of University of Wyoming, U.S.NCDC and CMA for providing long-term sounding data and surface observations, and also acknowledge the Ministry of Environment Protection of China and the US Embassy for providing API and $PM_{2.5}$ concentration data, respectively.

Competing interests

The authors declare that they have no conflict of interest.

Data availability

Radiosonde data during 1985–2014 were obtained from the University of Wyoming (http://weather.uwyo.edu/upperair/sounding.html). Hourly observations of surface air temperature during 30 years were extracted from ISD, provided by NCDC (ftp://ftp.ncdc.noaa.gov/pub/data/noaa). Dataset of daily precipitation during these 30 years were obtained from CMA website (http://data.cma.cn/data/detail/dataCode/SURF_CLI_CHN_MUL_DAY_CES_V3.0.html). API data during 2000–2012 and daily concentration of PM2.5 of Beijing in November to December during 2015–2017 were collected from Ministry of Environment Protection of the People's Republic of China (http://datacenter.mep.gov.cn). Hourly concentration data of $PM_{2.5}$ of Beijing in January of 2013 were collected from the US Embassy (http://www.stateair.net/web/historical/1/1.html).

Appendix A

Table A1. The information of 66 stations used in this study. Date ranges are the periods when radiosonde data, daily precipitation and daily maximum temperature are all available at the same time. The periods less than 30 years are highlighted in bold. The percentages of valid data are presented.

ID*	Name	Latitude (° N)	Longitude (° E)	Elevation (m)	Date Range	Valid Data
50527	Hailar	49.21	119.75	611	198501-201412	97.79%
50557	Nenjiang	49.16	125.23	243	198501-201412	98.88%
50953	Harbin	45.75	126.76	143	198501-201412	99.34%
51076	Altay	47.72	88.08	737	198501-201412	99.18%
51431	Yining	43.95	81.33	664	198501-201412	99.26%
51463	Urumqi	43.77	87.62	919	198501-201412	99.15%
51644	Kuqa	41.71	82.95	1100	198501-201412	99.32%
51709	Kashi	39.46	75.98	1291	198501-201412	99.17%
51777	Ruoqiang	39.02	88.16	889	198501-201412	99.09%
51828	Hotan	37.13	79.93	1375	198501-201412	99.34%
52203	Hami	42.81	93.51	739	198501-201412	99.27%
52418	Dunhuang	40.15	94.68	1140	198501-201412	99.05%
52533	Jiuquan	39.75	98.48	1478	198501-201412	98.87%
52681	Minqin	38.63	103.08	1367	198501-201412	98.46%
52818	Golmud	36.4	94.9	2809	198501-201412	99.17%
52836	Dulan	36.29	98.09	3192	198501-201412	96.88%
52866	Xining	36.71	101.75	2296	198501-201412	99.04%
53068	Erenhot	43.65	112	966	198501-201412	99.02%
53463	Hohhot	40.81	111.68	1065	198501-201412	99.25%
53614	Yinchuan	38.47	106.2	1112	198501-201412	98.17%
53772	Taiyuan	37.77	112.55	779	198501-201412	98.96%
53845	YanAn	36.59	109.5	959	198501-201412	99.32%
53915	Pingliang	35.54	106.66	1348	198501-201412	98.88%
54102	XilinHot	43.95	116.05	991	198501-201412	99.20%
54135	Tongliao	43.6	122.26	180	198501-201412	99.25%
54161	Changchun	43.9	125.21	238	198501-201412	98.98%
54218	Chifeng	42.25	118.95	572	198501-201412	99.26%
54292	Yanji	42.88	129.46	178	198501-201412	99.32%
54342	Shenyang	41.75	123.43	43	198501-201412	99.16%
54374	Linjiang	41.71	126.91	333	198501-201412	98.84%
54511	Beijing	39.93	116.28	55	198501-201412	99.25%

Table A1. Continued.

ID*	Name	Latitude (° N)	Longitude (° E)	Elevation (m)	Date Range	Valid Data
54662	Dalian	38.9	121.62	97	198501-201412	99.16%
55591	Lhasa	29.65	91.12	3650	198501-201412	97.72%
56029	Yushu	33	97.01	3682	198501-201412	97.11%
56080	Hezuo	35	102.9	2910	198501-201412	98.39%
56146	Garze	31.61	100	522	198501-201412	98.64%
56187	Wenjiang	30.7	103.83	541	**200501-201412**	98.03%
56571	Xichang	27.9	102.26	1599	198501-201412	98.65%
56739	Tengchong	25.11	98.48	1649	198501-201412	99.02%
56778	Kunming	25.01	102.68	1892	198501-201412	98.99%
56964	Simao	22.76	100.98	1303	198501-201412	99.24%
56985	Mengzi	23.38	103.38	1302	198501-201412	99.22%
57083	Zhengzhou	34.7	113.65	111	198501-201412	99.31%
57127	Hanzhong	33.06	107.02	509	198501-201412	99.34%
57131	Jinghe	34.26	108.58	411	**200710-201412**	99.92%
57447	Enshi	30.28	109.46	458	198501-201412	99.33%
57461	Yichang	30.7	111.3	134	198501-201412	99.31%
57494	Wuhan	30.61	114.12	23	198501-201412	99.32%
57516	Chongqing	29.51	106.48	260	**198708-201412**	98.56%
57816	Guiyang	26.47	106.65	1222	198501-201412	98.57%
57957	Guilin	25.33	110.3	166	198501-201412	99.33%
57993	Ganzhou	25.85	114.94	125	198501-201412	99.27%
58027	Xuzhou	34.27	117.15	42	198501-201412	99.33%
58238	Nanjing	32	118.8	7	198501-201412	99.34%
58362	Shanghai	31.4	121.46	4	**199106-201412**	98.88%
58424	Anqing	30.53	117.05	20	198501-201412	99.33%
58457	Hangzhou	30.22	120.16	43	198501-201412	99.05%
58606	Nanchang	28.6	115.91	50	198501-201412	99.31%
58633	QuXian	28.95	118.86	71	198501-201412	99.03%
58847	Fuzhou	26.07	119.27	85	198501-201412	99.24%
59134	Xiamen	24.47	118.08	139	198501-201412	99.29%
59211	Baise	23.9	106.6	175	198501-201412	99.15%
59265	Wuzhou	23.48	111.3	120	198501-201412	98.29%
59316	Shantou	23.35	116.66	3	198501-201412	99.23%
59431	Nanning	22.62	108.2	126	198501-201412	99.28%
59758	Haikou	20.03	110.34	24	198501-201412	99.13%

* World Meteorological Organization Identification Number.

References:

Ao, C. O., Waliser, D. E., Chan, S. K., Li, J.-L., Tian, B., Xie, F., and Mannucci, A. J.: Planetary boundary layer heights from GPS radio occultation refractivity and humidity profiles, Journal of Geophysical Research-Atmospheres, 117, doi:10.1029/2012jd017598, 2012.

Beyrich, F.: Mixing height estimation from sodar data - A critical discussion, Atmospheric Environment, 31, 3941-3953, doi:10.1016/s1352-2310(97)00231-8, 1997.

Bianco, L., and Wilczak, J. M.: Convective boundary layer depth: Improved measurement by Doppler radar wind profiler using fuzzy logic methods, Journal of Atmospheric and Oceanic Technology, 19, 1745-1758, 2002.

Blanchard, D. O.: Assessing the vertical distribution of convective available potential energy, Weather and Forecasting, 13, 870-877, doi:10.1175/1520-0434(1998)013<0870:atvdoc>2.0.co;2, 1998.

Bressi, M., Sciare, J., Ghersi, V., Bonnaire, N., Nicolas, J. B., Petit, J. E., Moukhtar, S., Rosso, A., Mihalopoulos, N., and Feron, A.: A one-year comprehensive chemical characterisation of fine aerosol (PM2.5) at urban, suburban and rural background sites in the region of Paris (France), Atmospheric Chemistry and Physics, 13, 7825-7844, doi:10.5194/acp-13-7825-2013, 2013.

Cai, W., Li, K., Liao, H., Wang, H., and Wu, L.: Weather conditions conducive to Beijing severe haze more frequent under climate change, Nature Climate Change, 7, 257-262, 2017.

Chan, C. K., and Yao, X.: Air pollution in mega cities in China, Atmospheric Environment, 42, 1-42, doi:10.1016/j.atmosenv.2007.09.003, 2008.

Chen, H. P., and Wang, H. J.: Haze Days in North China and the associated atmospheric circulations based on daily visibility data from 1960 to 2012, Journal of Geophysical Research-Atmospheres, 120, 5895-5909, doi:10.1002/2015jd023225, 2015.

Chen, J., Zhao, C. S., Ma, N., Liu, P. F., Goebel, T., Hallbauer, E., Deng, Z. Z., Ran, L., Xu, W. Y., Liang, Z., Liu, H. J., Yan, P., Zhou, X. J., and Wiedensohler, A.: A parameterization of low visibilities for hazy days in the North China Plain, Atmospheric Chemistry and Physics, 12, 4935-4950, doi:10.5194/acp-12-4935-2012, 2012.

Chen, J.-L., Xiao, B.-B., Chen, C.-D., Wen, Z.-F., Jiang, Y., Lv, M.-Q., Wu, S.-J., and Li, G.-S.: Estimation of monthly-mean global solar radiation using MODIS atmospheric product over China, Journal of Atmospheric and Solar-Terrestrial Physics, 110, 63-80, doi:10.1016/j.jastp.2014.01.017, 2014.

Chen, Y., and Xie, S.: Temporal and spatial visibility trends in the Sichuan Basin, China, 1973 to 2010, Atmospheric Research, 112, 25-34, doi:10.1016/j.atmosres.2012.04.009, 2012.

Coen, M. C., Praz, C., Haefele, A., Ruffieux, D., Kaufmann, P., and Calpini, B.: Determination and climatology of the planetary boundary layer height above the Swiss plateau by in situ and remote sensing measurements as well as by the COSMO-2 model, Atmospheric Chemistry and Physics, 14, 13205-13221, doi:10.5194/acp-14-13205-2014, 2014.

Dawson, J. P., Bloomer, B. J., Winner, D. A., and Weaver, C. P.: Understanding the meteorological drivers of US particulate matter concentrations in a changing climate, Bulletin of the American Meteorological Society, 95, 521-532, 2014.

Deser, C., Tomas, R., Alexander, M., and Lawrence, D.: The seasonal atmospheric response to projected Arctic

sea ice loss in the late 21st century, J. Climate, 23, 333–351, 2010.

Domroes, M., Peng, G.: The climate of China. Springer, Berlin Heidelberg, New York, 361pp., 1988.

Elminir, H. K.: Dependence of urban air pollutants on meteorology, Science of the Total Environment, 350, 225-237, doi:10.1016/j.scitodenv.2005.01.043, 2005.

Eresmaa, N., Karppinen, A., Joffre, S. M., Rasanen, J., and Talvitie, H.: Mixing height determination by ceilometer, Atmospheric Chemistry and Physics, 6, 1485-1493, 2006.

Frederick, K. L., Edward, J. T., and Dennis, G. T.: The atmosphere: an introduction to meteorology, Prentice Hall, New Jersey, USA, 528 pp., 2012.

Frueh, B., and Wirth, V.: Convective Available Potential Energy (CAPE) in mixed phase cloud conditions, Quarterly Journal of the Royal Meteorological Society, 133, 561-569, doi:10.1002/qj.39, 2007.

Fu, G. Q., Xu, W. Y., Yang, R. F., Li, J. B., and Zhao, C. S.: The distribution and trends of fog and haze in the North China Plain over the past 30 years, Atmospheric Chemistry and Physics, 14, 11949-11958, doi:10.5194/acp-14-11949-2014, 2014.

Guo, S., Hu, M., Zamora, M. L., Peng, J., Shang, D., Zheng, J., Du, Z., Wu, Z., Shao, M., Zeng, L., Molina, M. J., and Zhang, R.: Elucidating severe urban haze formation in China, Proceedings of the National Academy of Sciences of the United States of America, 111, 17373-17378, doi:10.1073/pnas.1419604111, 2014.

Han, Z., Zhou, B., Xu, Y., Wu, J., and Shi, Y.: Projected changes in haze pollution potential in China: an ensemble of regional climate model simulations, Atmospheric Chemistry and Physics, 17, 10109-10123, 2017.

He, K., Yang, F., Ma, Y., Zhang, Q., Yao, X., Chan, C. K., Cadle, S., Chan, T., and Mulawa, P.: The characteristics of PM2. 5 in Beijing, China, Atmospheric Environment, 35, 4959-4970, 2001.

Holton, J. R.: A introduction to dynamic meteorology International Geophysics Series, vol. 48. Academic press, London, 511 pp., 1992.

Holzworth, G. C.: Estimates of mean maximum mixing depths in the contiguous United States, Mon. Weather Rev, 92, 235-242, 1964.

Holzworth, G. C.: Mixing depths, wind speeds and air pollution potential for selected locations in the United States, Journal of applied Meteorology, 6, 1039-1044, 1967.

Holzworth, G. C.: Mixing heights, wind speeds, and potential for urban air pollution throughout the contiguous United States, US Government Printing Office, 1972.

Horton, D.E., Skinner, C.B., Singh, D., and Diffenbaugh, N.S.: Occurrence and persistence of future atmospheric stagnation events, Nature Climate Change, 4, 698–703, doi:10.1038/NCLIMATE2272, 2014.

Huang, Q., Cai, X., Song, Y., and Zhu, T.: Air stagnation in China (1985–2014): climatological mean features and trends, Atmospheric Chemistry and Physics, 17, 7793-7805, 2017.

Huang, R.-J., Zhang, Y., Bozzetti, C., Ho, K.-F., Cao, J.-J., Han, Y., Daellenbach, K. R., Slowik, J. G., Platt, S. M., and Canonaco, F.: High secondary aerosol contribution to particulate pollution during haze events in China, Nature, 514, 218-222, 2014.

Jacob, D.J., and Winner, D.A.: Effect of climate change on air quality. Atmos. Environ., 43, 51–63, doi:10.1016/j.atmosenv.2008.09.051, 2009.

Ji, D., Li, L., Wang, Y., Zhang, J., Cheng, M., Sun, Y., Liu, Z., Wang, L., Tang, G., and Hu, B.: The heaviest particulate air-pollution episodes occurred in northern China in January, 2013: Insights gained from

observation, Atmospheric Environment, 92, 546-556, 2014.

Ji, D., Wang, Y., Wang, L., Chen, L., Hu, B., Tang, G., Xin, J., Song, T., Wen, T., and Sun, Y.: Analysis of heavy pollution episodes in selected cities of northern China, Atmospheric Environment, 50, 338-348, 2012.

Jordan, N. S., Hoff, R. M., and Bacmeister, J. T.: Validation of Goddard Earth Observing System - version 5 MERRA planetary boundary layer heights using CALIPSO, Journal of Geophysical Research: Atmospheres, 115, 2010.

Korshover, J.: Climatology of stagnating anticyclones east of the Rocky Mountains, 1936–1965 (Association of stagnating anticyclones with incidents of heavy air pollution in eastern United States from 1936 to 1965), 1967.

Korshover, J. and Angell, J.K.: A Review of Air-Stagnation Cases in the Eastern United States During 1981—Annual Summary, Mon. Wea. Rev., 110, 1515–1518, doi: 10.1175/1520-0493(1982)110<1515:AROASC>2.0.CO;2, 1982.

Leibensperger, E. M., Mickley, L. J., and Jacob, D. J.: Sensitivity of US air quality to mid-latitude cyclone frequency and implications of 1980–2006 climate change, Atmospheric Chemistry and Physics, 8, 7075-7086, 2008.

Lelieveld, J., Evans, J. S., Fnais, M., Giannadaki, D., and Pozzer, A.: The contribution of outdoor air pollution sources to premature mortality on a global scale, Nature, 525, 367-+, doi:10.1038/nature15371, 2015.

Leung, L.R. and Gustafson, W.I.: Potential regional climate change and implications to US air quality, Geophys. Res. Lett., 32, 367–384, doi:10.1029/2005GL022911, 2005.

Li, X., Xia, X., Wang, L., Cai, R., Zhao, L., Feng, Z., Ren, Q., and Zhao, K.: The role of foehn in the formation of heavy air pollution events in Urumqi, China, J. Geophys. Res.: Atmos., 120, 5371–5384, doi:10.1002/2014JD022778, 2015.

Li, L., Qian, J., Ou, C.-Q., Zhou, Y.-X., Guo, C., and Guo, Y.: Spatial and temporal analysis of Air Pollution Index and its timescale-dependent relationship with meteorological factors in Guangzhou, China, 2001–2011, Environmental Pollution, 190, 75-81, 2014.

Liao, H., Chen, W. T., and Seinfeld, J. H.: Role of climate change in global predictions of future tropospheric ozone and aerosols, J. Geophys. Res.-Atmos., 111, doi:10.1029/2005JD006852, 2006.

Liu, J., Huang, J., Chen, B., Zhou, T., Yan, H., Jin, H., Huang, Z., and Zhang, B.: Comparisons of PBL heights derived from CALIPSO and ECMWF reanalysis data over China, Journal of Quantitative Spectroscopy and Radiative Transfer, 153, 102-112, 2015.

Liu, S., and Liang, X.-Z.: Observed diurnal cycle climatology of planetary boundary layer height, Journal of Climate, 23, 5790-5809, 2010.

Liu, X. G., Li, J., Qu, Y., Han, T., Hou, L., Gu, J., Chen, C., Yang, Y., Liu, X., Yang, T., Zhang, Y., Tian, H., and Hu, M.: Formation and evolution mechanism of regional haze: a case study in the megacity Beijing, China, Atmospheric Chemistry and Physics, 13, 4501-4514, doi:10.5194/acp-13-4501-2013, 2013.

Lokoshchenko, M. A.: Long-term sodar observations in Moscow and a new approach to potential mixing determination by radiosonde data, Journal of Atmospheric and oceanic Technology, 19, 1151-1162, 2002.

Lu, Z., Zhang, Q., and Streets, D. G.: Sulfur dioxide and primary carbonaceous aerosol emissions in China and India, 1996-2010, Atmospheric Chemistry and Physics, 11, 9839-9864, doi:10.5194/acp-11-9839-2011, 2011.

Mamtimin, B. and Meixner, F.X.: The characteristics of air pollution in the semi-arid city of Urumqi (NW China) and its relation to climatological process, Geophys. Res. Abstr., 9, 06537, 2007.

Markowski, P., and Richardson, Y.: Mesoscale meteorology in midlatitudes, John Wiley & Sons, 2011.

Miller, M. E.: Forecasting afternoon mixing depths and transport wind speeds, Monthly Weather Review, 95, 35-44, 1967.

Monkam, D.: Convective available potential energy (CAPE) in northern Africa and tropical Atlantic and study of its connections with rainfall in Central and West Africa during Summer 1985, Atmospheric Research, 62, 125-147, doi:10.1016/s0169-8095(02)00006-6, 2002.

Murugavel, P., Pawar, S. D., and Gopalakrishnan, V.: Trends of Convective Available Potential Energy over the Indian region and its effect on rainfall, International Journal of Climatology, 32, 1362-1372, doi:10.1002/joc.2359, 2012.

Myoung, B., and Nielsen-Gammon, J. W.: Sensitivity of Monthly Convective Precipitation to Environmental Conditions, Journal of Climate, 23, 166-188, doi:10.1175/2009jcli2792.1, 2010.

Patil, M., Patil, S., Waghmare, R., and Dharmaraj, T.: Planetary Boundary Layer height over the Indian subcontinent during extreme monsoon years, Journal of Atmospheric and Solar-Terrestrial Physics, 92, 94-99, 2013.

Peel, M. C., Finlayson, B. L., and McMahon, T. A.: Updated world map of the Köppen-Geiger climate classification, Hydrology and earth system sciences discussions, 4, 439-473, 2007.

Pei, L., Yan, Z., Sun, Z., Miao, S., and Yao, Y.: Increasing persistent haze in Beijing: potential impacts of weakening East Asian winter monsoons associated with northwestern Pacific sea surface temperature trends, Atmospheric Chemistry and Physics, 18, 3173-3183, 2018.

Peng, J. F., Hu, M., Guo, S., Du, Z. F., Zheng, J., Shang, D. J., Zamora, M. L., Zeng, L. M., Shao, M., Wu, Y. S., Zheng, J., Wang, Y., Glen, C. R., Collins, D. R., Molina, M. J., and Zhang, R. Y.: Markedly enhanced absorption and direct radiative forcing of black carbon under polluted urban environments, Proceedings of the National Academy of Sciences of the United States of America, 113, 4266-4271, doi:10.1073/pnas.1602310113, 2016.

Quan, J., Zhang, Q., He, H., Liu, J., Huang, M., and Jin, H.: Analysis of the formation of fog and haze in North China Plain (NCP), Atmospheric Chemistry and Physics, 11, 8205-8214, 2011.

Ran, L., Zhao, C. S., Xu, W. Y., Lu, X. Q., Han, M., Lin, W. L., Yan, P., Xu, X. B., Deng, Z. Z., Ma, N., Liu, P. F., Yu, J., Liang, W. D., and Chen, L. L.: VOC reactivity and its effect on ozone production during the HaChi summer campaign, Atmos. Chem. Phys., 11, 4657–4667, doi:10.5194/acp-11-4657-2011, 2011.

Riemann-Campe, K., Blender, R., and Fraedrich, K.: Global memory analysis in observed and simulated CAPE and CIN, International Journal of Climatology, 31, 1099-1107, doi:10.1002/joc.2148, 2011.

Riemann-Campe, K., Fraedrich, K., and Lunkeit, F.: Global climatology of Convective Available Potential Energy (CAPE) and Convective Inhibition (CIN) in ERA-40 reanalysis, Atmospheric Research, 93, 534-545, doi:10.1016/j.atmosres.2008.09.037, 2009.

Rigby, M., and Toumi, R.: London air pollution climatology: indirect evidence for urban boundary layer height and wind speed enhancement, Atmospheric Environment, 42, 4932-4947, 2008.

Romatschke, U., Medina, S., and Houze, R. A., Jr.: Regional, Seasonal, and Diurnal Variations of Extreme

Convection in the South Asian Region, Journal of Climate, 23, 419-439, doi:10.1175/2009jcli3140.1, 2010.

Schiemann, R., Lüthi, D., and Schär, C.: Seasonality and interannual variability of the westerly jet in the Tibetan Plateau region, Journal of Climate, 22, 2940-2957, 2009.

Seibert, P., Beyrich, F., Gryning, S.-E., Joffre, S., Rasmussen, A., and Tercier, P.: Review and intercomparison of operational methods for the determination of the mixing height, Atmospheric environment, 34, 1001-1027, 2000.

Seidel, D. J., Ao, C. O., and Li, K.: Estimating climatological planetary boundary layer heights from radiosonde observations: Comparison of methods and uncertainty analysis, Journal of Geophysical Research: Atmospheres, 115, 2010.

Seidel, D. J., Fu, Q., Randel, W. J., and Reichler, T. J.: Widening of the tropical belt in a changing climate, Nat. Geosci., 1, 21–24, https://doi.org/10.1038/ngeo.2007.38, 2008.

Seidel, D. J., Zhang, Y., Beljaars, A., Golaz, J. C., Jacobson, A. R., and Medeiros, B.: Climatology of the planetary boundary layer over the continental United States and Europe, Journal of Geophysical Research: Atmospheres, 117, 2012.

Stull, R.B.: An Introduction to Boundary Layer Meteorology. Kluwer Academic Publishers, Dordrecht, The Netherlands, 1988.

Sun, Y., Jiang, Q., Wang, Z., Fu, P., Li, J., Yang, T., and Yin, Y.: Investigation of the sources and evolution processes of severe haze pollution in Beijing in January 2013, Journal of Geophysical Research: Atmospheres, 119, 4380-4398, 2014.

Tai, A. P. K., Mickley, L. J., and Jacob, D. J.: Correlations between fine particulate matter (PM2.5) and meteorological variables in the United States: Implications for the sensitivity of PM2.5 to climate change, Atmospheric Environment, 44, 3976-3984, doi:10.1016/j.atmosenv.2010.06.060, 2010.

Tompkins, A. M., and Craig, G. C.: Radiative–convective equilibrium in a three‐dimensional cloud‐ensemble model, Quarterly Journal of the Royal Meteorological Society, 124, 2073-2097, 1998.

Tucker, S. C., Senff, C. J., Weickmann, A. M., Brewer, W. A., Banta, R. M., Sandberg, S. P., Law, D. C., and Hardesty, R. M.: Doppler lidar estimation of mixing height using turbulence, shear, and aerosol profiles, Journal of Atmospheric and Oceanic Technology, 26, 673-688, 2009.

van der Kamp, D., and McKendry, I.: Diurnal and seasonal trends in convective mixed-layer heights estimated from two years of continuous ceilometer observations in Vancouver, BC, Boundary-layer meteorology, 137, 459-475, 2010.

van Donkelaar, A., Martin, R. V., Brauer, M., Kahn, R., Levy, R., Verduzco, C., and Villeneuve, P. J.: Global Estimates of Ambient Fine Particulate Matter Concentrations from Satellite-Based Aerosol Optical Depth: Development and Application, Environmental Health Perspectives, 118, 847-855, doi:10.1289/ehp.0901623, 2010.

von Engeln, A., and Teixeira, J.: A planetary boundary layer height climatology derived from ECMWF reanalysis data, Journal of Climate, 26, 6575-6590, 2013.

Wang, H.-J., and Chen, H.-P.: Understanding the recent trend of haze pollution in eastern China: roles of climate change, Atmospheric Chemistry and Physics, 16, 4205-4211, 2016.

Wang, H. J., Chen, H. P., and Liu, J. P.: Arctic sea ice decline intensified haze pollution in eastern China, Atmos.

Ocean. Sci. Lett., 8, 1–9, 2015.

Wang, J.X.L. and Angell, J.K.: Air stagnation climatology for the United States, NOAA/Air Resource Laboratory ATLAS, 1999.

Wang, X., Dickinson, R. E., Su, L., Zhou, C., and Wang, K.: PM2.5 Pollution in China and How It Has Been Exacerbated by Terrain and Meteorological Conditions, Bulletin of the American Meteorological Society, doi:10.1175/bams-d-16-0301.1, 2017.

Wang, Y., Zhang, Y., Hao, J., and Luo, M.: Seasonal and spatial variability of surface ozone over China: Contributions from background and domestic pollution, Atmos. Chem. Phys., 11, 3511–3525, doi:10.5194/acp-11-3511-2011, 2011.

Wehner, B., and Wiedensohler, A.: Long term measurements of submicrometer urban aerosols: statistical analysis for correlations with meteorological conditions and trace gases, Atmospheric Chemistry and Physics, 3, 867-879, 2003.

Williams, E., and Renno, N.: An analysis of the conditional instability of the tropical atmosphere, Monthly Weather Review, 121, 21-36, 1993.

World Health Organization (WHO) (2005) Air quality guidelines for particulate matter, ozone, nitrogen dioxide and sulfur dioxide. Global update 2005, http://www.who.int/phe/health_topics/outdoorair/outdoorair_aqg/en/. Accessed 18 Nov 2017

Xie, F., Wu, D., Ao, C., Mannucci, A., and Kursinski, E.: Advances and limitations of atmospheric boundary layer observations with GPS occultation over southeast Pacific Ocean, Atmospheric Chemistry and Physics, 12, 903-918, 2012.

Ye, X. X., Song, Y., Cai, X. H., and Zhang, H. S.: Study on the synoptic flow patterns and boundary layer process of the severe haze events over the North China Plain in January 2013, Atmospheric Environment, 124, 129-145, doi:10.1016/j.atmosenv.2015.06.011, 2016.

Yin, Z., Wang, H., and Chen, H.: Understanding severe winter haze events in the North China Plain in 2014: roles of climate anomalies, Atmospheric Chemistry and Physics, 17, 1641, 2017.

Zhang, Y., Wen, X. Y., and Jang, C. J.: Simulating chemistry-aerosol-cloud-radiation-climate feedbacks over the continental US using the online-coupled Weather Research Forecasting Model with chemistry (WRF/Chem), Atmospheric Environment, 44, 3568-3582, doi:10.1016/j.atmosenv.2010.05.056, 2010.

Zhu, X., He, H., Liu, M., Yu, G., Sun, X., and Gao, Y.: Spatio-temporal variation of photosynthetically active radiation in China in recent 50 years, Journal of Geographical Sciences, 20, 803-817, 2010.

Figure Captions

Figure 1. The relationship between air pollution index (API) and 500 hPa wind speeds in most polluted days (i.e., days when API ranks in the 90th percentile or higher) in boreal winter half-year (October–March) during 2000–2012 of Beijing station. Air pollutions are classified into six levels (I–VI) which means excellent, good, lightly polluted, moderately polluted, heavily polluted, and severely polluted conditions, respectively.

Figure 2. Topography of China and locations of 66 stations analyzed in this study. Cross marks indicate the four representative stations: Harbin, Urumqi, Beijing and Chongqing.

Figure 3. The spatial distribution of daily maximal ventilation (a), MMD (b) and transport wind speed (c) averaged over 30 years (1985–2014).

Figure 4. Annual cycle of ventilation, MMD and transport wind speed of four representative stations (Harbin, Urumqi, Beijing and Chongqing). Monthly mean values are given as horizontal bars in the middle, 25% and 75% percentiles are shown as boxes' lower and upper boundaries, and 10% and 90% percentiles as lower and upper whiskers.

Figure 5. The spatial distribution of annual precipitation (a) and precipitation days (b) during 1985–2014.

Figure 6. Annual cycle of precipitation (a) and precipitation days (b) of four representative stations (Harbin, Urumqi, Beijing and Chongqing).

Figure 7. The spatial distribution of annual mean CAPE (a), CIN (b) and real latent instability (c) during 1985–2014.

Figure 8. Annual cycle of CAPE (black line) and CIN (green line) values of four representative stations (Harbin, Urumqi, Beijing and Chongqing). The orange filled area indicates values of CAPE with CIN deducted, i.e., real latent instability.

Figure 9. The spatial distribution of annual mean stagnation days (a), stagnation cases (b) and duration of stagnation cases (c) under new metrics.

Figure 10. Annual cycles of air stagnation days and cases of four representative stations (Harbin, Urumqi, Beijing and Chongqing), as well as the national average values. Black and grey lines indicate stagnation conditions under the BSI and ASI metrics, respectively. Solid and dash lines represents stagnation days and cases, respectively.

Figure 11. Monthly variations of API averaged over 13 years (2000–2012), as well as the corresponding air stagnation days under the ASI and BSI criteria. Blue line: ASI; red line: BSI. Monthly mean values of API are given as horizontal bars in the middle, 25% and 75% percentiles are shown as boxes' lower and upper boundaries, and 10% and 90% percentiles as lower and upper whiskers.

Figure 12. Correlations between monthly mean API and the total air stagnation days in the corresponding month in China winter half-year (October–March) during 2000–2012. R stands for correlation coefficient. Blue: ASI; red: BSI.

Figure 13. Time series of ASI and BSI with hourly concentration of $PM_{2.5}$ during January 2013 of Beijing (a), and the corresponding variation of main components of ASI and BSI, i.e., daily ventilation and 500 hPa and 10 m wind speeds (b).

Figure 14. Time series of 24-h averaged concentration of $PM_{2.5}$ of Beijing from November to December during 2015–2017. Stagnation days under ASI and BSI metric are marked with stripes and grey colors, respectively.

Figure 15. Averaged concentration of $PM_{2.5}$ during November and December in 2015, 2016 and 2017, and the corresponding number of boundary-layer stagnation days.

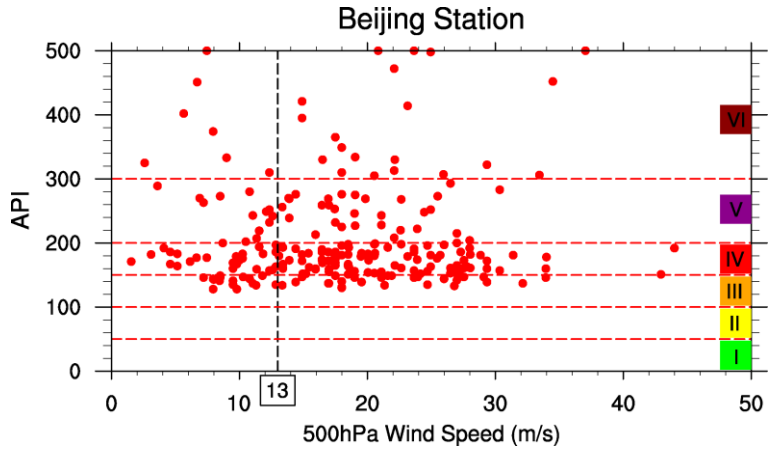

Figure 1. The relationship between air pollution index (API) and 500 hPa wind speeds in most polluted days (i.e., days when API ranks in the 90th percentile or higher) in boreal winter half-year (October–March) during 2000–2012 of Beijing station. Air pollutions are classified into six levels (I–VI) which means excellent, good, lightly polluted, moderately polluted, heavily polluted, and severely polluted conditions, respectively.

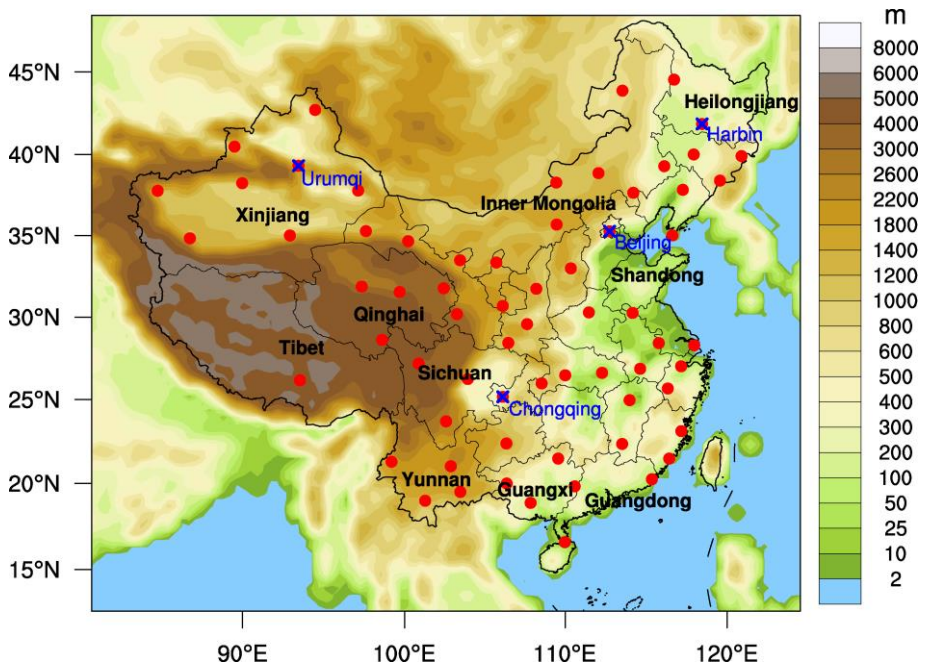

Figure 2. Topography of China and locations of 66 stations analyzed in this study. Cross marks indicate the four representative stations: Harbin, Urumqi, Beijing and Chongqing.

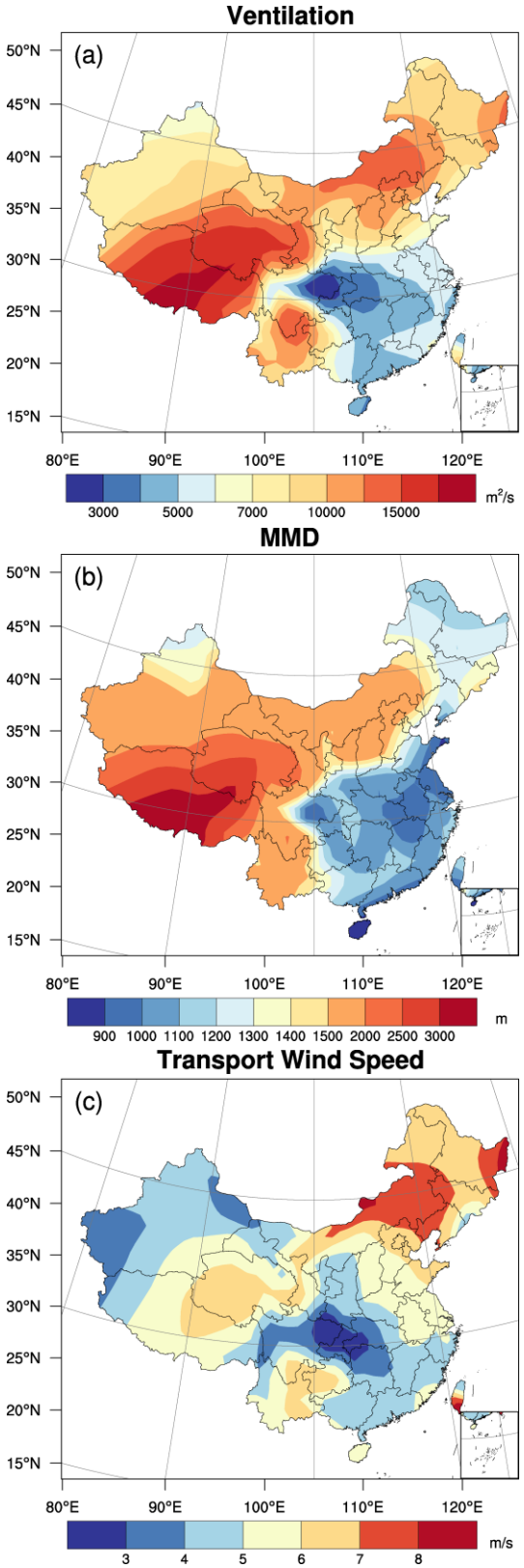

Figure 3. The spatial distribution of daily maximal ventilation (a), MMD (b) and transport wind speed (c) averaged over 30 years (1985–2014).

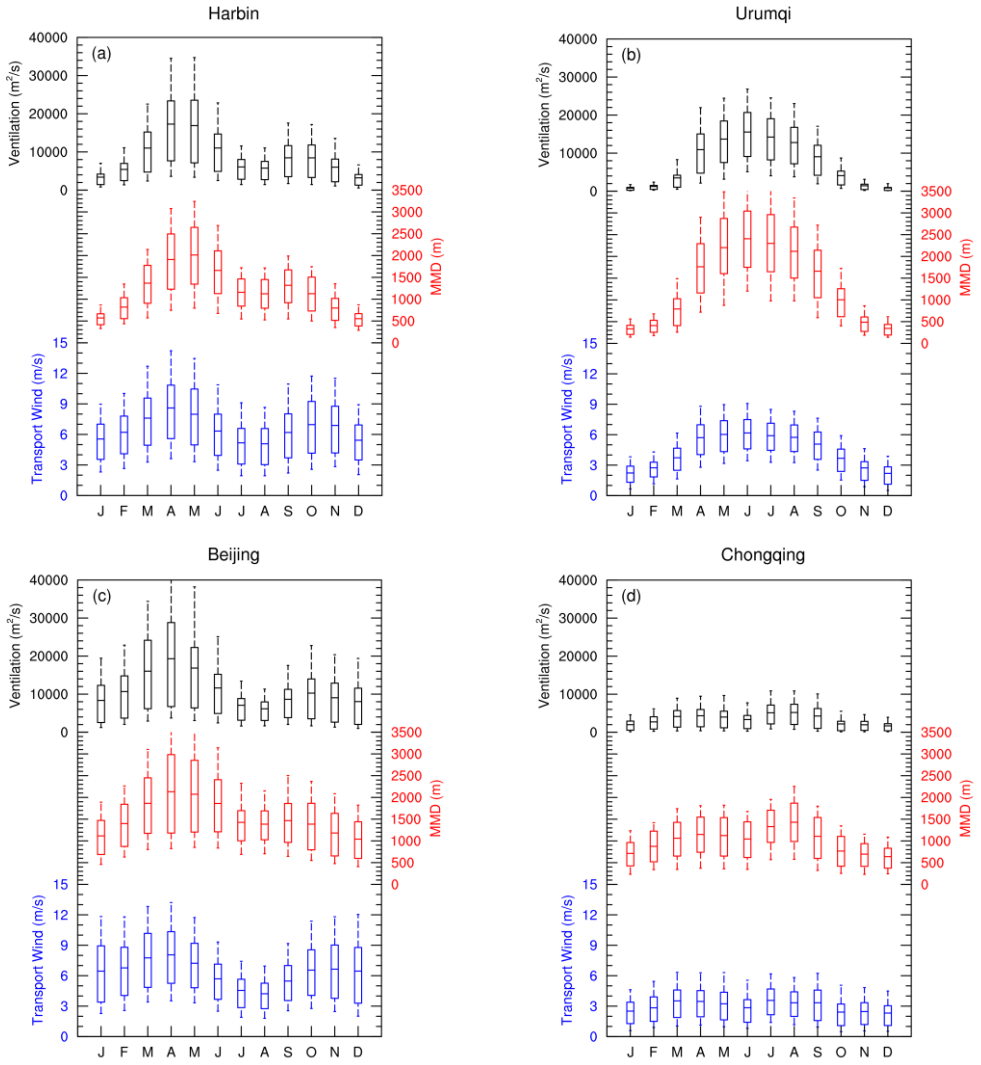

Figure 4. Annual cycle of ventilation, MMD and transport wind speed of four representative stations (Harbin, Urumqi, Beijing and Chongqing). Monthly mean values are given as horizontal bars in the middle, 25% and 75% percentiles are shown as boxes' lower and upper boundaries, and 10% and 90% percentiles as lower and upper whiskers.

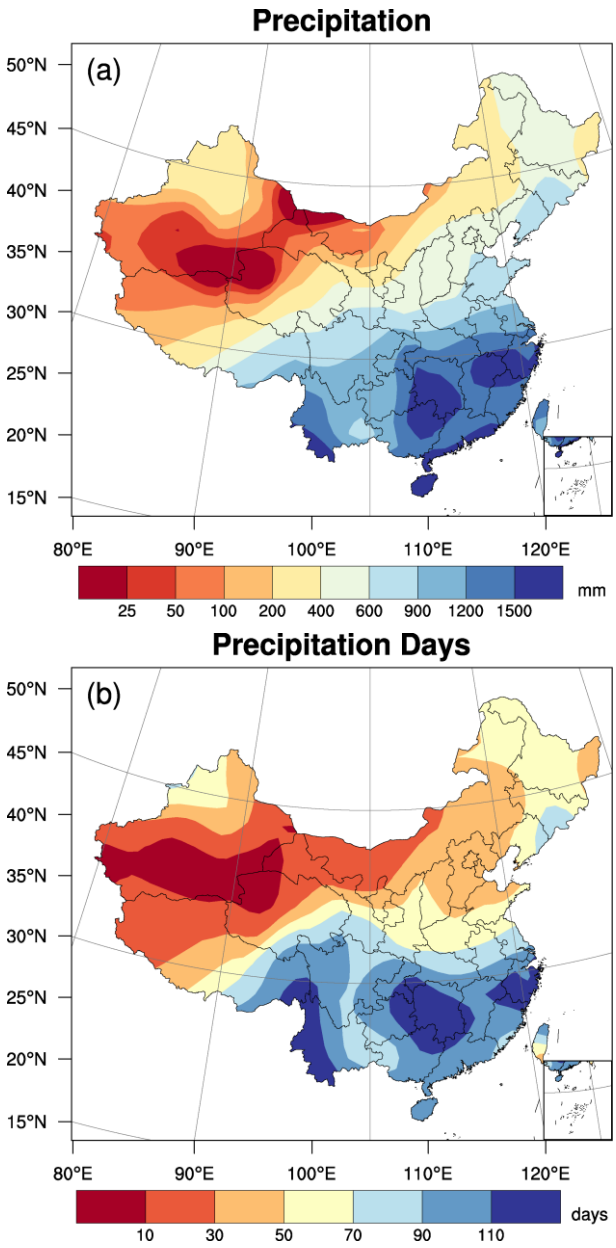

Figure 5. The spatial distribution of annual precipitation (a) and precipitation days (b) during 1985–2014.

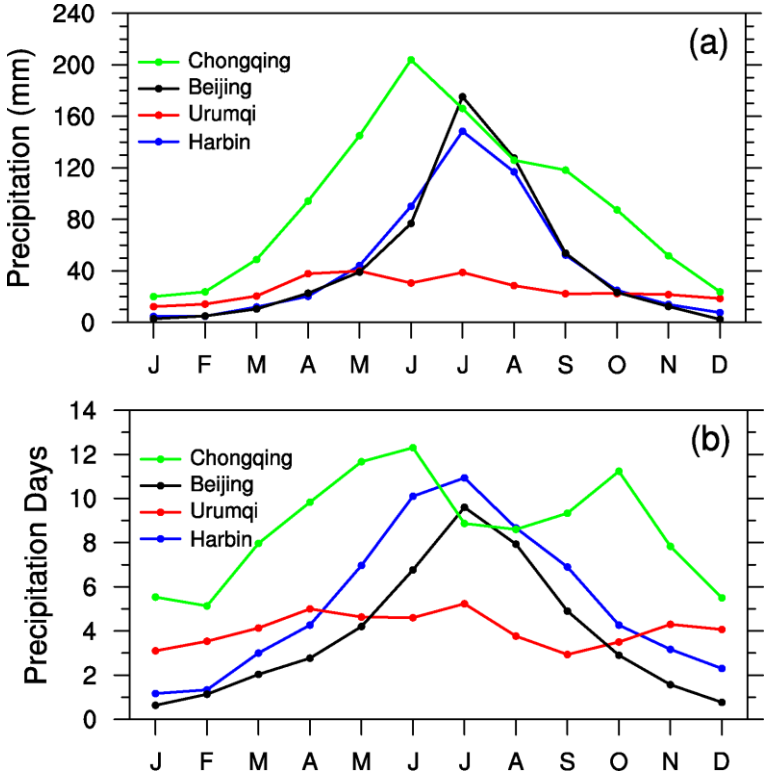

Figure 6. Annual cycle of precipitation (a) and precipitation days (b) of four representative stations (Harbin, Urumqi, Beijing and Chongqing).

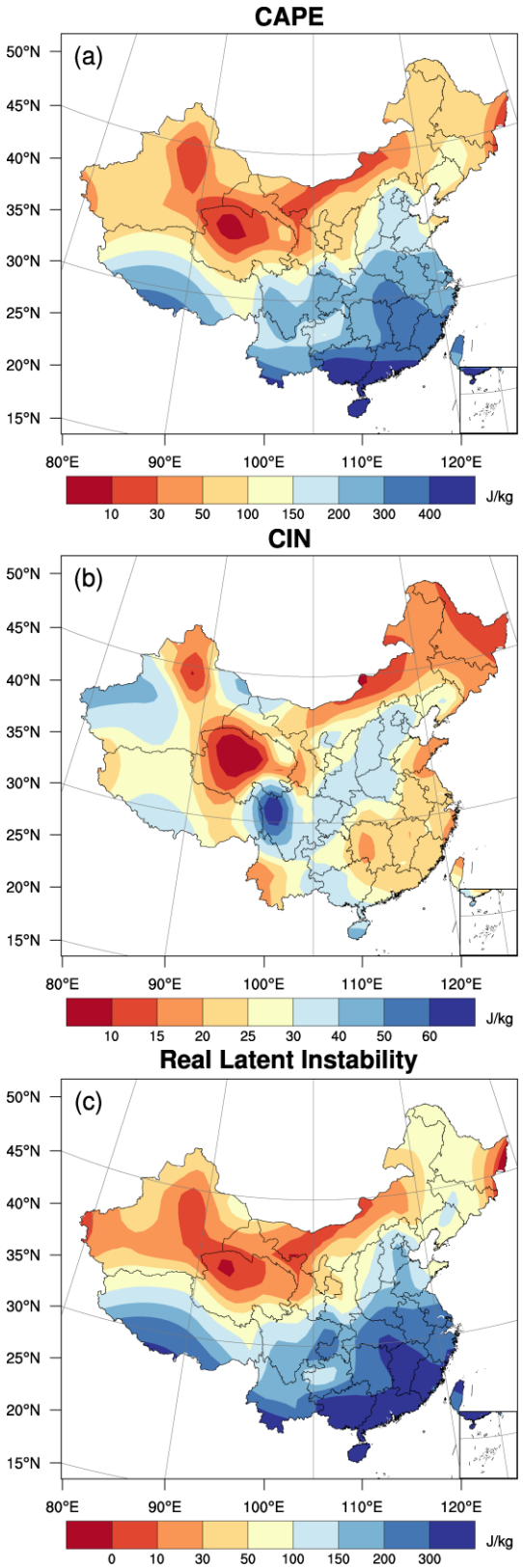

Figure 7. The spatial distribution of annual mean CAPE (a), CIN (b) and real latent instability (c) during 1985–2014.

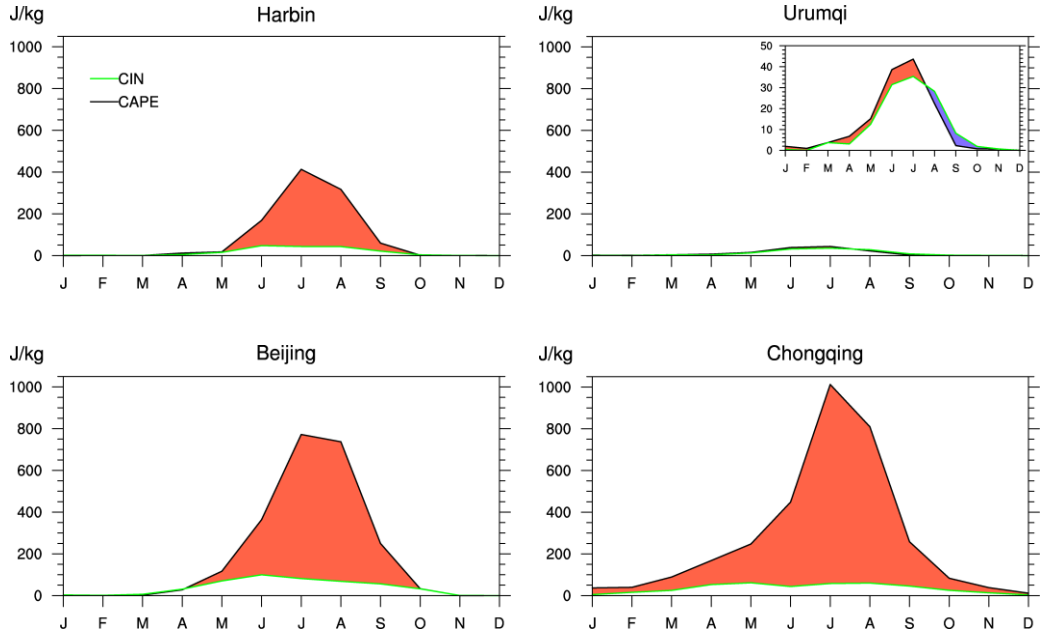

Figure 8. Annual cycle of CAPE (black line) and CIN (green line) values of four representative stations (Harbin, Urumqi, Beijing and Chongqing). The orange filled area indicates values of CAPE with CIN deducted, i.e., real latent instability.

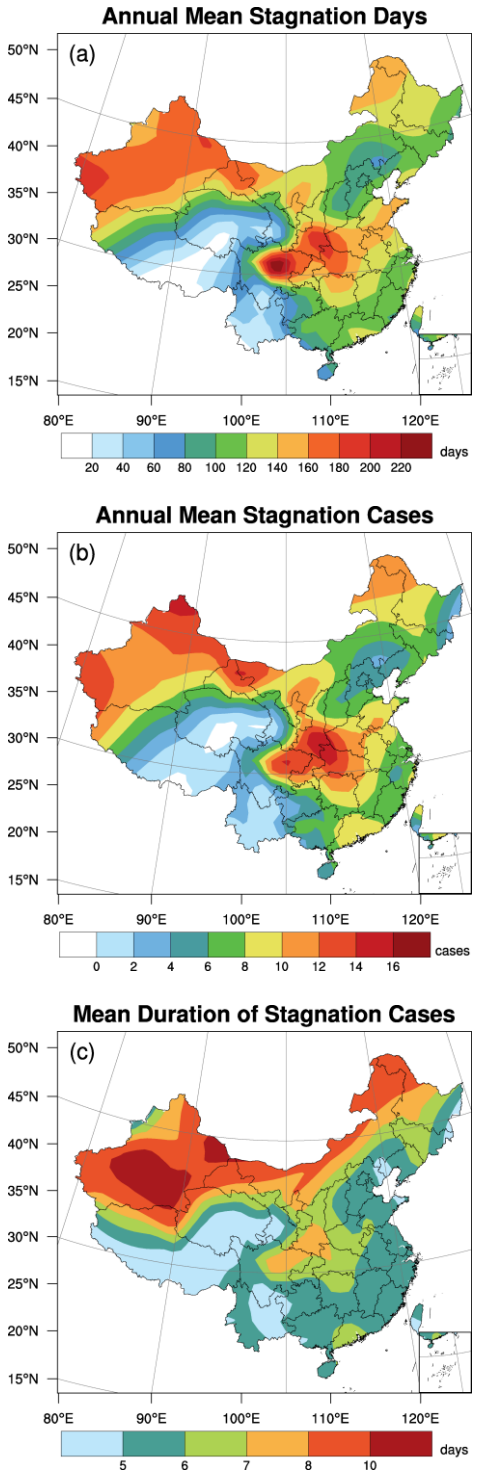

Figure 9. The spatial distribution of annual mean stagnation days (a), stagnation cases (b) and duration of stagnation cases (c) under new metrics.

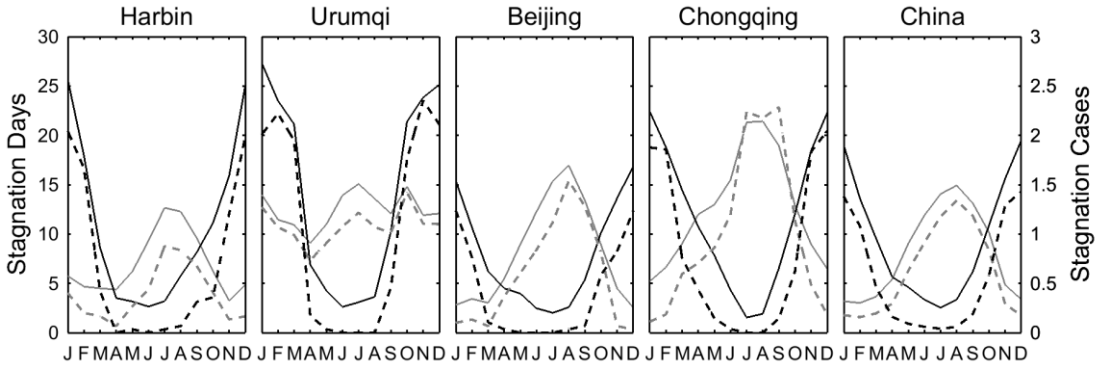

Figure 10. Annual cycles of air stagnation days and cases of four representative stations (Harbin, Urumqi, Beijing and Chongqing), as well as the national average values. Black and grey lines indicate stagnation conditions under the BSI and ASI metrics, respectively. Solid and dash lines represents stagnation days and cases, respectively.

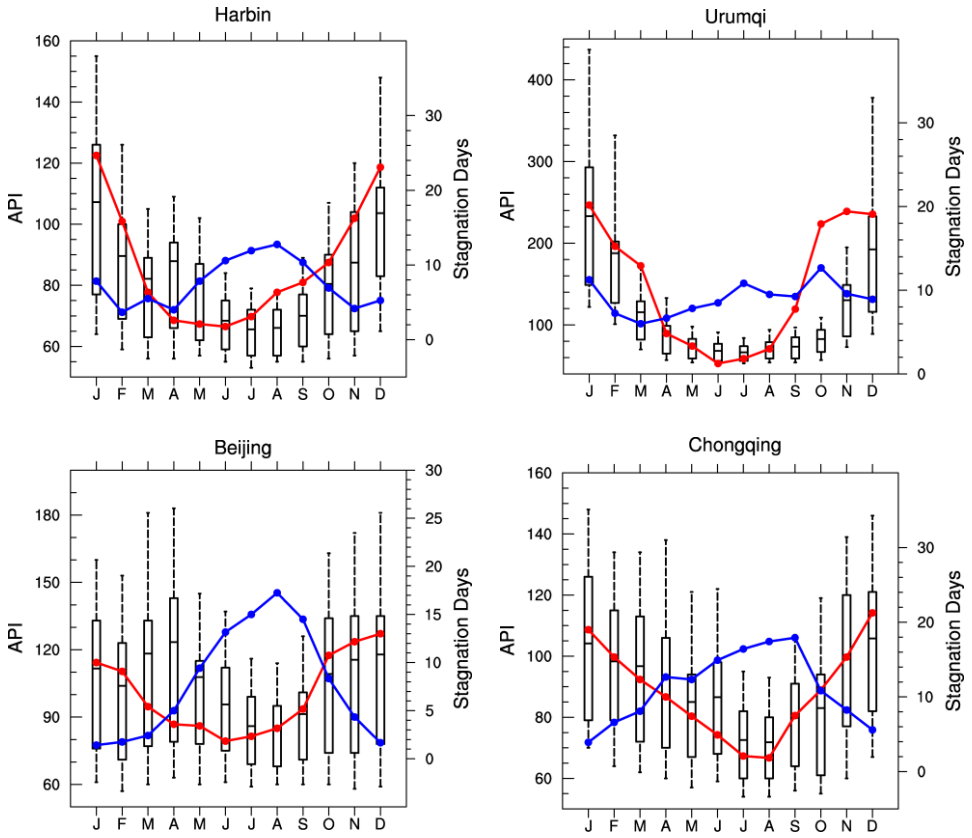

Figure 11. Monthly variations of API averaged over 13 years (2000–2012), as well as the corresponding air stagnation days under the ASI and BSI criteria. Blue line: ASI; red line: BSI. Monthly mean values of API are given as horizontal bars in the middle, 25% and 75% percentiles are shown as boxes' lower and upper boundaries, and 10% and 90% percentiles as lower and upper whiskers.

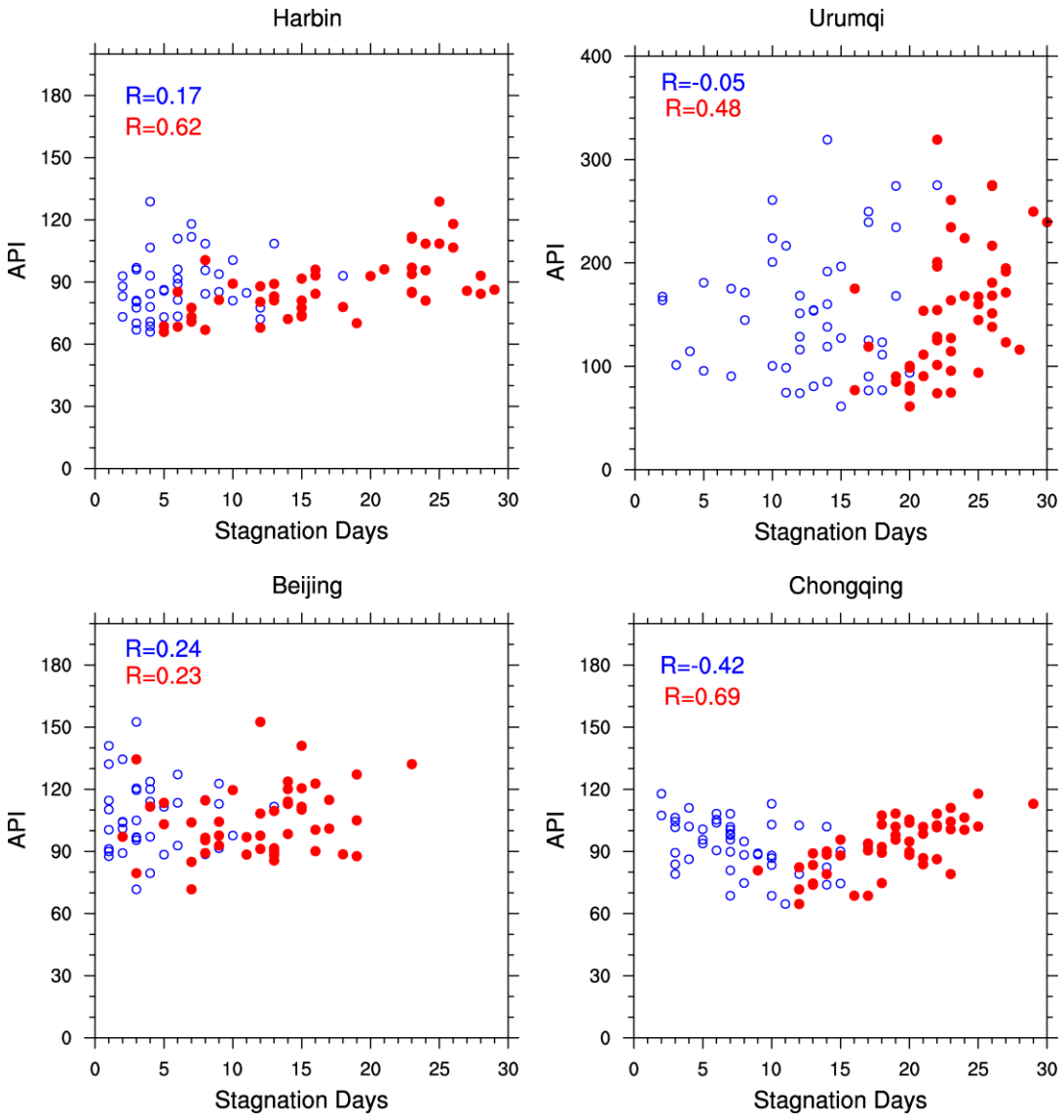

Figure 12. Correlations between monthly mean API and the total air stagnation days in the corresponding month in China winter half-year (October–March) during 2000–2012. R stands for correlation coefficient. Blue: ASI; red: BSI.

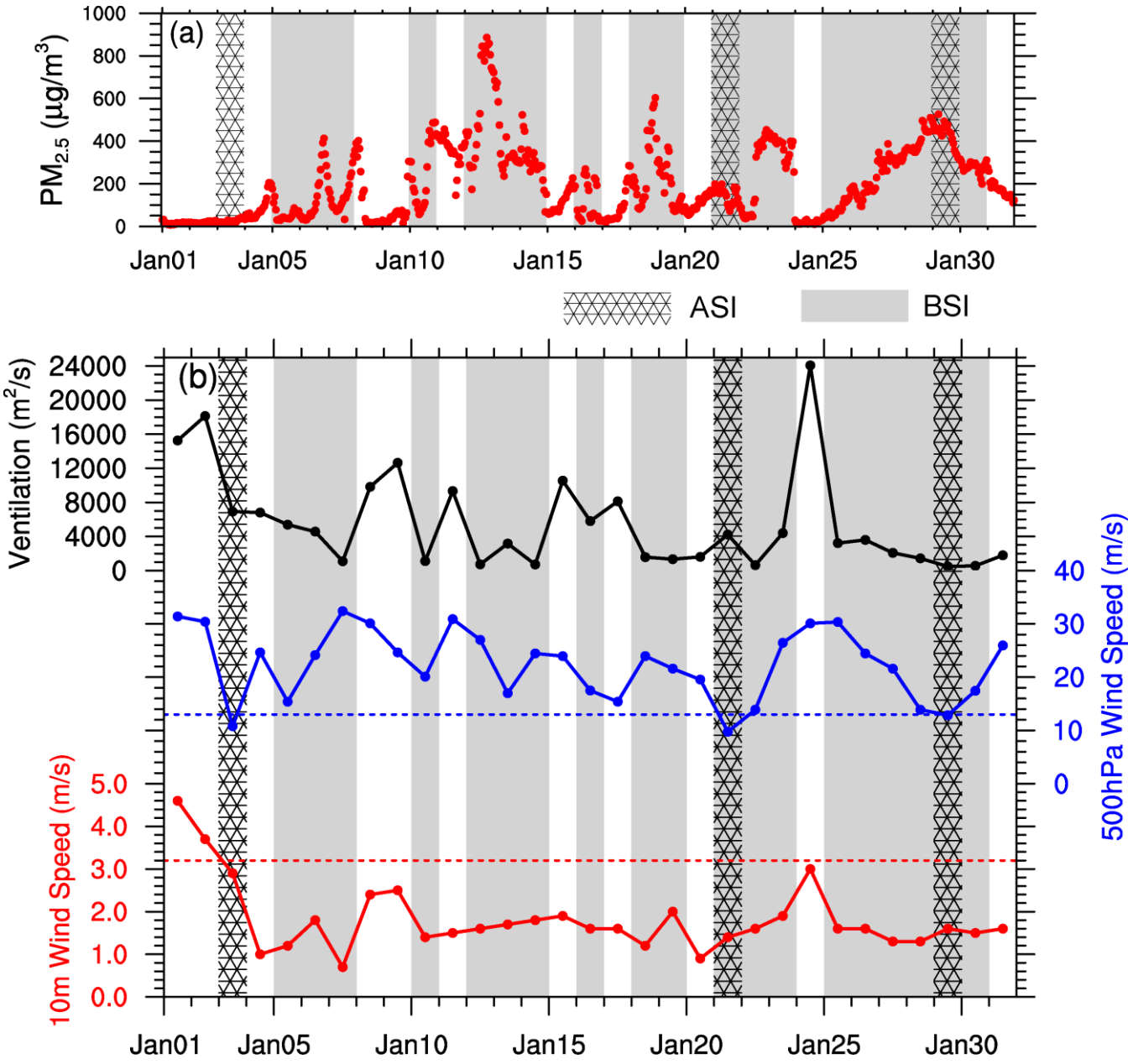

Figure 13. Time series of ASI and BSI with hourly concentration of $PM_{2.5}$ during January 2013 of Beijing (a), and the corresponding variation of main components of ASI and BSI, i.e., daily ventilation and 500 hPa and 10 m wind speeds (b).

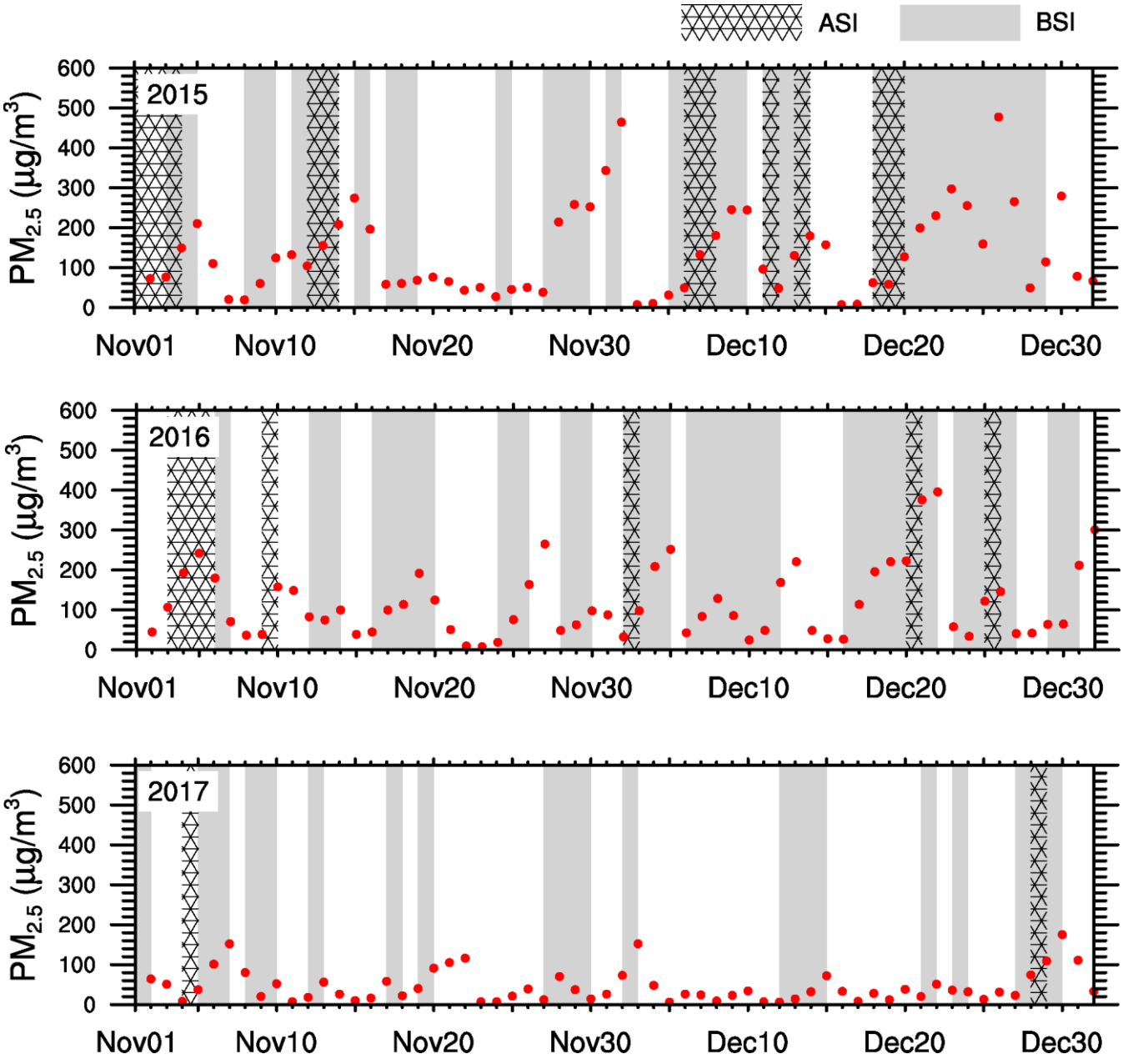

Figure 14. Time series of 24-h averaged concentration of $PM_{2.5}$ of Beijing from November to December during 2015–2017. Stagnation days under ASI and BSI metric are marked with stripes and grey colors, respectively.

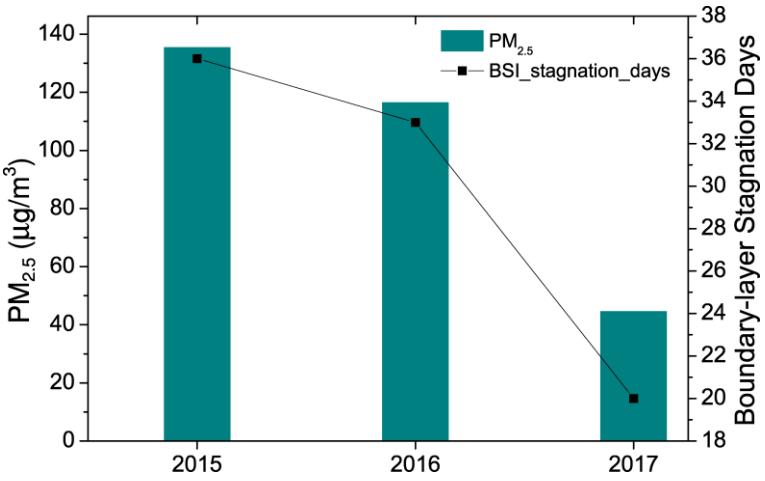

Figure 15. Averaged concentration of $PM_{2.5}$ during November and December in 2015, 2016 and 2017, and the corresponding number of boundary-layer stagnation days.

Table

Table 1. Dependence of BSI on its components, i.e. daily precipitation, ventilation and CAPE. [a]

Station	Month	Standardized Partial Regression Coefficients (β)			R^2
		Precipitation	Ventilation	CAPE_CIN	
Harbin	Jan.	0.22	1.00	-0.02	0.99
	Apr.	0.58	0.84	-0.13	0.74
	Jul.	0.30	0.57	0.48	0.70
	Oct.	0.37	0.98	0.01	0.95
Urumqi	Jan.	0.17	1.00	-0.03	0.99
	Apr.	0.23	1.04	0.10	0.89
	Jul.	0.36	0.83	0.40	0.77
	Oct.	0.33	0.91	0.12	0.95
Beijing	Jan.	0.30	1.06	0.04	0.98
	Apr.	0.45	0.85	0.05	0.82
	Jul.	0.07	0.33	0.70	0.47
	Oct.	0.26	0.85	0.19	0.80
Chongqing	Jan.	0.21	0.63	0.36	0.98
	Apr.	0.32	0.56	0.38	0.89
	Jul.	0.21	-0.02	0.75	0.67
	Oct.	0.35	0.25	0.68	0.84

[a] The relationships between monthly stagnation days and its corresponding components were derived by using multiple linear regression analysis. “Precipitation” stands for number of days with no precipitation; “Ventilation” for number of days when daily maximum ventilation is less than 6000 m^2/s; “CAPE_CIN” for number of days when the value of CAPE is less than the absolute value of CIN.

Table 2. How many days are identified as air stagnation days in each API category?

API Classification	Harbin		Urumqi		Beijing		Chongqing	
	BSI	ASI	BSI	ASI	BSI	ASI	BSI	ASI
0-50	---[a]	---	---	---	---	---	---	---
51-100	30.5%	28.1%	31.1%	39.7%	20.1%	31.6%	37.1%	45.7%
101-150	64.4%	24.6%	79.4%	35.7%	35.2%	34.3%	59.7%	41.9%
151-200	87.2%	23.4%	87.9%	42.8%	45.4%	27.5%	64.9%	52.7%
201-300	70.0%	30.0%	91.8%	47.5%	49.3%	16.4%	50.0%	25.0%
301-500	28.6%	28.6%	89.9%	56.9%	41.4%	13.8%	---	---

[a] The result is ignored because there are less than 5 days falling into this category.